Hindawi
International Journal of Atmospheric Sciences
Volume 2017, Article ID 9251034, 30 pages
https://doi.org/10.1155/2017/9251034

Research Article

Radiation Transfer Calculations and Assessment of Global Warming by CO_2

Hermann Harde

Experimental Physics and Materials Science, Helmut-Schmidt-University, Holstenhofweg 85, 22043 Hamburg, Germany

Correspondence should be addressed to Hermann Harde; harde@hsu-hh.de

Received 29 June 2016; Revised 3 October 2016; Accepted 1 November 2016; Published 20 March 2017

Academic Editor: Bin Yu

We present detailed line-by-line radiation transfer calculations, which were performed under different atmospheric conditions for the most important greenhouse gases water vapor, carbon dioxide, methane, and ozone. Particularly cloud effects, surface temperature variations, and humidity changes as well as molecular lineshape effects are investigated to examine their specific influence on some basic climatologic parameters like the radiative forcing, the long wave absorptivity, and back-radiation as a function of an increasing CO_2 concentration in the atmosphere. These calculations are used to assess the CO_2 global warming by means of an advanced two-layer climate model and to disclose some larger discrepancies in calculating the climate sensitivity. Including solar and cloud effects as well as all relevant feedback processes our simulations give an equilibrium climate sensitivity of $C_S = 0.7^{\circ}C$ (temperature increase at doubled CO_2) and a solar sensitivity of $S_S = 0.17^{\circ}C$ (at 0.1% increase of the total solar irradiance). Then CO_2 contributes 40% and the Sun 60% to global warming over the last century.

1. Introduction

The Fifth Assessment Report (AR5) [1] of the Intergovernmental Panel on Climate Change (IPCC), a list of all abbreviations is found in the annex, announces new evidence of an anthropogenic climate change based on many independent scientific analyses from observations of the climate system, paleoclimate archives, theoretical studies of climate processes, and simulations using climate models. So, the IPCC classifies the human influence as extremely likely to be the dominant cause of the observed warming since the mid-20th century (AR5-WG1-SPM-D3). Increasing emissions of carbon dioxide (CO_2) over the last century especially are made responsible for this change, and the equilibrium climate sensitivity (ECS or C_S) as a measure for the Earth's temperature increase at doubled CO_2 concentration in the atmosphere is specified to be likely in the range 1.5°C to 4.5°C (high confidence) (AR5-WG1-SPM, p16).

Although in all these fields of climate sciences great progress has been achieved over the last decades and our knowledge about the Earth-atmosphere system (EASy) could significantly be improved, explanations of the observed global warming over the last century in particular the anthropogenic contributions to this warming are still quite contradictorily discussed.

All the more it is surprising

(i) that many of the consulted analyses and also the AR5 itself do not better and clearly distinguish between an anthropogenic emission of CO_2 and a naturally generated part, where the latter even contributes more than 95% to the overall emission, and its generation rate and the respective absorption rate sensitively respond on global temperature variations;

(ii) that the IPCC claims it would be extremely likely that more than half of the observed increase in global average surface temperature from 1951 to 2010 was caused by the anthropogenic increase in greenhouse gas concentrations and other anthropogenic forcings, while contributions from natural forcing and an internal variability both would only likely be in the range of −0.1°C to 0.1°C;

(iii) that the meanwhile well known delayed response of CO_2 and methane (CH_4) to sea and air temperature changes (see, e.g., Petit et al. [2]; Monnin et al. [3];

Caillon et al. [4]; Torn and Harte [5]; Humlum et al. [6]; Salby [7]) are not considered in AR5, and respective consequences for an anthropogenic global warming are not discussed;

(iv) that quite uncertain data about cloud feedbacks and studies of the radiative forcing (RF) of greenhouse (GH) gases are referred, which are mostly valid for clear sky conditions, while the introduction of clouds is usually omitted (AR5-WG1- Chap.8.3.1);

(v) that the IPCC denies any noticeable solar influence on the actual climate, although strong evidence of an increasing solar activity over the last century exists (see, e.g., Hoyt & Schatten [8]; Willson & Mordvinov [9]; Shapiro et al. [10]; Ziskin & Shaviv [11]; Scafetta & Willson [12]; Usoskin et al. [13]; Zhao & Feng [14]; Soon et al. [15]);

(vi) that obviously important effects like convection and evaporation feedback, which can contribute to significant negative feedback (Harde-2014 [16]), are not considered in many analyses.

Nevertheless, despite these deficits and simplifications the mean equilibrium climate sensitivity is specified with high confidence, and the GH gases are even assigned with very high confidence (95%) to be responsible for the actual climate changes.

Here we will focus on the assessment of one of the most important quantities in climate sciences and its validation, the ECS, which has to be scrutinized in more detail. Due to its far reaching consequences for future climate predictions it is particularly important to understand and to discover the large discrepancies between different accounting methods applied for this quantity. Also the weighting of some quite different and even counteracting processes which control our climate, but which are not always well understood, has carefully to be investigated with its implications on the climate sensitivity. A quite critical report of actually published ECS values and accounting methods expanded in AR5 has been published by Lewis and Crok [17].

In this contribution we will also retrace the main steps of the IPCC's preferred accounting system and compare this with our own advanced two-layer climate model (2LCM), which is especially appropriate to calculate the influence of increasing CO_2 concentrations on global warming as well as the impact of solar variations on the climate (Harde-2014 [16]). This model describes the atmosphere and the ground as two layers acting simultaneously as absorbers and Planck radiators, and it includes additional heat transfer between these layers due to convection and evaporation. It also considers short wave (sw) and long wave (lw) scattering processes at the atmosphere and at clouds; it includes all common feedback processes like water vapor, lapse rate, and albedo feedback but additionally takes into account temperature dependent sensible and latent heat fluxes as well as temperature induced and solar induced cloud cover feedback.

The objective of our studies is not to present a new only "true ECS" but to identify some of the different assumptions and approximations with their far reaching consequences in climate politics. It is without any doubt that the ECS is the most important measure for the CO_2 influence on our climate, but it is also clear that this quantity does not distinguish between anthropogenic and natural CO_2 emissions. Therefore, as long as any natural variations in the CO_2 concentrations are not accurately known, the ECS cannot be used as a reliable indicator only for an anthropogenic global warming. All this in mind the reader may have his own reservations about the published data for this measure and its significance for a man-made climate change.

For the assessment of the ECS the IPCC favors the concept of radiative forcing (RF), which is supposed to be appropriate to describe the transition of the surface-troposphere system from one equilibrium state to another in response to an externally imposed perturbation. Therefore, in Section 2 we briefly outline some basic relations characterizing this concept, before we present in Section 3 detailed line-by-line radiation transfer (LBL-RT) calculations for the lw up- and downwelling fluxes in the atmosphere (for details see Harde [16, 18, 19]), this for clear sky, global mean cloud cover, full cloudiness, different surface temperatures, humidity, and even different lineshapes. These calculations were performed for the most important GH gases water vapor (WV), carbon dioxide, methane, and ozone and are based on the HITRAN08 database [20]. Since the concentration of the GH gases and the atmospheric pressure are changing with temperature and altitude, the atmosphere has to be segmented into up to 228 sublayers from ground to 86 km height and in some cases additionally into three climate zones. When these computations are repeated for different CO_2 concentrations at otherwise same conditions, from the changing fluxes on the one hand the CO_2 initiated RF as the main parameter for the IPCC accounting scheme and on the other hand the sw and lw absorptivities as well as the back-radiated fraction of the atmospheric emission as the key parameters in our 2LCM can be derived.

Section 4 summarizes the main features of the 2LCM and its calibration to satellite data, for the radiation and heat fluxes using the well known radiation and energy budget scheme of Trenberth et al. [21], for temperature changes due to cloud cover variations applying the observations within the International Satellite Cloud Climatology Project (ISCCP) [22]. With the respective key parameters of Section 3 integrated in the climate model we simulate the Earth's surface temperature and the lower tropospheric temperature as a function of the CO_2 concentration. The temperature increase at doubled CO_2 concentration then directly gives the CO_2 climate sensitivity. Such simulations reproduce the direct or basic ECS value (without feedback processes), as specified by the IPCC, within better than 10%. Significant differences, however, can be observed with the different feedback effects included. Our investigations show the largest discrepancies for the WV and cloud feedback, but they also disclose the importance of one of the primary stabilizers of the whole climate system, the evaporation feedback. Therefore, these processes and their contributions are extensively analyzed under different humidity, surface temperature, lapse rate, and cloud cover conditions.

In particular, these studies show that the observed cloud changes within the ISCCP cannot exclusively be explained by pure thermally induced cloud cover changes but obviously are additionally controlled by a further cloud forcing mechanism. Since there exists strong evidence that the solar activity also has a powerful influence on the cloud cover, it is reasonable to postulate such a solar induced cloud feedback (see, e.g., Svensmark [23]; Haigh [24]). This is investigated in detail in Section 5, differentiating between a pure thermal impact of an increasing solar activity and a nonthermally induced solar cloud feedback. An important criterion for a validation, which mechanism might control such cloud changes, can be derived from model simulations, which include the solar anomaly over the last century and compare this directly with the observed global warming over this period. These investigations indicate that due to the strong cloud feedback the observed warming over the last century can only satisfactorily be explained, attributing a significant fraction to the increased solar activity over this period (see also Ziskin & Shaviv [11]; Vahrenholt & Lüning [25]).

Our simulations predict a solar contribution of about 60% and a CO_2 induced contribution of 40% to global warming over the last century with an equilibrium climate sensitivity of 0.7°C, which is almost a factor of five smaller than published in AR5.

2. Radiative Forcing

The concept of RF is well established in climate sciences and used to assess the global warming as a result of an external perturbation of EASy (AR5-WG1-Chap.8). This perturbation can result from solar anomalies, from increased GH gas concentrations or volcanic activities. In all cases a direct proportionality of the Earth's temperature increase ΔT_E as response to an external forcing ΔF is assumed in the form

$$\Delta T_E = \lambda_S \cdot \Delta F, \tag{1}$$

with λ_S as the climate sensitivity parameter, also known as Planck sensitivity. The negative reciprocal of λ_S is called the Planck feedback (see AR5-WG1-Chap.9), although this is not a feedback process in the common sense like the water vapor, the albedo, or lapse rate feedback, which all describe an internal amplification or attenuation of an external perturbation. The Planck feedback rather represents the change of the outgoing long wave radiation (OLR), or more precisely the change of the total upwelling lw intensity $I^{\mathrm{up}}_{\mathrm{total}}$ with the ground temperature. Since an increasing amount of OLR with the temperature causes a negative feedback for EASy, it can be defined as the negative partial derivative as follows:

$$-\frac{\partial \mathrm{OLR}}{\partial T_E} = -\frac{\partial I^{\mathrm{up}}_{\mathrm{total}}}{\partial T_E} = \frac{1}{\lambda_S}. \tag{2a}$$

Its value, deduced as an average from different climate models, is given in AR5-WG1-Tab.9.5 as $-3.2\,\mathrm{W/m^2/^\circ C}$, and, thus, the Planck sensitivity becomes $\lambda_S = 0.31\,\mathrm{W^{-1}\,m^2\,^\circ C}$. A somewhat simplified method to assess the Planck feedback and sensitivity, which agrees within 15% with these values, is to use the slope of the Stefan-Boltzmann law at an effective Earth temperature $T_{\mathrm{eff}} = 255$ K and emissivity $\varepsilon_{\mathrm{eff}} = 1$ with

$$-\left.\frac{\partial I^{\mathrm{up}}_{\mathrm{total}}}{\partial T_A}\right|_{T_{\mathrm{eff}}=255\,\mathrm{K}} = -4\varepsilon_{\mathrm{eff}}\sigma T^3_{\mathrm{eff}} = -\frac{4I^{\mathrm{up}}_{\mathrm{total}}}{T_{\mathrm{eff}}} \Longrightarrow \frac{1}{\lambda_S} \tag{2b}$$

and to assume the same temperature response for the surface as for the atmosphere. This results in a Planck feedback of $-3.76\,\mathrm{W/m^2/^\circ C}$ and a climate sensitivity parameter $\lambda_S = 0.27\,\mathrm{W^{-1}\,m^2\,^\circ C}$. σ is the Stefan-Boltzmann constant with $5.67{\cdot}10^{-8}\,\mathrm{W/m^2/^\circ C^4}$ and $I^{\mathrm{up}}_{\mathrm{total}}$ the OLR with $239.4\,\mathrm{W/m^2}$.

Eq. (1) is the basis for many climate models (see AR4 [26] and AR5 [1]) and even for more complex models like the Atmosphere-Ocean-General-Circulation Models (AOGCMs) this fundamental relation is used to express the influence of the growing GH gas concentrations on the surface temperature. So, for these models and also for the observationally based energy budget ECS estimates (see, e.g., Forster & Gregory [27]; Lindzen & Choi [28]) ΔF is a quite fundamental quantity, which cannot directly be measured but has to be deduced from extensive spectroscopic calculations or solar data, which on their part rely on many individual observations and measurements. For quite actual investigations of ΔF see also Feldman et al. [29].

In this context it should be noticed that alternative definitions of RF have been developed, each with its own advantages and limitations (see AR5-WG1-Chap.8). Here we only consider the instantaneous RF, which refers to an instantaneous change in the net (down minus up) radiative flux (sw plus lw) due to an imposed change. This forcing is usually defined in terms of flux changes at the top of the atmosphere (TOA) or at the tropopause.

In this contribution, particularly the influence of CO_2 on global warming is of interest. Therefore, in the next subsection we present some actual radiation transfer (RT) calculations, from which the instantaneous RF due to increasing CO_2 in the atmosphere and also some related quantities, which are of relevance for our two-layer climate model, can be derived. Since for these model calculations it is not sufficient only to consider the net radiative fluxes at the tropopause, neglecting the downwelling absorption changes in the troposphere and the upwelling absorption changes over the stratosphere, we apply the RT concept from the surface to TOA and vice versa. The sw absorption changes over the full atmosphere and this as a function of the CO_2 concentration can be captured from our previous investigations (Harde-2014 [16]).

As already outlined, an important reference for the influence of CO_2 is the temperature increase at doubled CO_2 concentration under steady state conditions, which is known as the equilibrium climate sensitivity ECS or C_S, and the respective lw forcing may be designated as $\Delta F_{2\times CO_2}$. Since at TOA a lw downwelling flux is zero, the forcing at TOA can be defined as difference of the total outgoing intensities $I^{\mathrm{up}}_{\mathrm{total}}$ at single and doubled CO_2 concentration C:

$$\Delta F_{2\times \mathrm{CO}_2} = I^{\mathrm{up}}_{\mathrm{total}}(C) - I^{\mathrm{up}}_{\mathrm{total}}(2C), \tag{3}$$

where here we primarily consider the lw radiative forcing. $I^{\mathrm{up}}_{\mathrm{total}}$ can be explained to consist of the nonabsorbed terrestrial intensity ($I_E - I_{\mathrm{abs}}$) plus the emitted intensity of the atmosphere in upward direction I^{up}_A; thus, it holds the following:

$$\begin{aligned}\Delta F_{2\times \mathrm{CO}_2} &= I_E - I_{\mathrm{abs}}(C) + I^{\mathrm{up}}_A(C) - I_E + I_{\mathrm{abs}}(2C) \\ &\quad - I^{\mathrm{up}}_A(2C) \\ &= \Delta I^{\mathrm{up}}_A - \Delta I_{\mathrm{abs}}\end{aligned} \tag{4}$$

with

$$\begin{aligned}\Delta I^{\mathrm{up}}_A &= I^{\mathrm{up}}_A(C) - I^{\mathrm{up}}_A(2C), \\ \Delta I_{\mathrm{abs}} &= I_{\mathrm{abs}}(C) - I_{\mathrm{abs}}(2C).\end{aligned} \tag{5}$$

I_E is the intensity of the incident terrestrial radiation and I_{abs} the absorbed flux in the atmosphere.

So, due to (4) this forcing generally consists of two contributions, the change in the upward atmospheric emission and the change in the atmospheric absorption of terrestrial radiation, both as response to a doubling of the CO_2 concentration.

Expressing the downwelling atmospheric intensity I^{down}_A via the total emitted intensity I^{total}_A and the fraction f_A, which is directed downward (also called asymmetry factor of the emitted atmospheric radiation) and which is generally found from integrating the respective spectral intensities $I^{\mathrm{up,down}}_{A,\tilde{\nu}}$ at TOA and the surface over the frequency or reciprocal wavelength (wavenumber) $\tilde{\nu}$ with

$$f_A = \frac{I^{\mathrm{down}}_A}{I^{\mathrm{total}}_A} = \frac{\int_0^\infty I^{\mathrm{down}}_{A,\tilde{\nu}} d\tilde{\nu}}{\int_0^\infty I^{\mathrm{down}}_{A,\tilde{\nu}} d\tilde{\nu} + \int_0^\infty I^{\mathrm{up}}_{A,\tilde{\nu}} d\tilde{\nu}}, \tag{6}$$

the difference $\Delta I^{\mathrm{down}}_A$ between single and doubled concentration gives

$$\begin{aligned}\Delta I^{\mathrm{down}}_A &= I^{\mathrm{down}}_A(C) - I^{\mathrm{down}}_A(2C) \\ &= I^{\mathrm{total}}_A(C)\cdot f_A(C) - I^{\mathrm{total}}_A(2C)\cdot f_A(2C) \\ &= I^{\mathrm{total}}_A(C)\cdot f_A(C) - \left(I^{\mathrm{total}}_A(C) - \Delta I^{\mathrm{total}}_A\right) \\ &\quad \cdot \left(f_A(C) - \Delta f_A\right) \\ &= I^{\mathrm{total}}_A(C)\cdot \Delta f_A + \Delta I^{\mathrm{total}}_A \cdot f_A(C) - \Delta I^{\mathrm{total}}_A \\ &\quad \cdot \Delta f_A,\end{aligned} \tag{7}$$

with $\Delta I^{\mathrm{total}}_A$ and Δf_A as the respective differences of I^{total}_A and f_A at single and doubled CO_2 concentration.

Then, with (7), for the difference of the upwelling atmospheric intensities we can write

$$\begin{aligned}\Delta I^{\mathrm{up}}_A &= I^{\mathrm{total}}_A(C)\cdot\left(1 - f_A(C)\right) - I^{\mathrm{total}}_A(2C) \\ &\quad \cdot \left(1 - f_A(2C)\right) \\ &= I^{\mathrm{total}}_A(C) - I^{\mathrm{total}}_A(2C) - I^{\mathrm{total}}_A(C)\cdot f_A(C) \\ &\quad + I^{\mathrm{total}}_A(2C)\cdot f_A(2C) \\ &= \Delta I^{\mathrm{total}}_A - I^{\mathrm{total}}_A(C)\cdot \Delta f_A - \Delta I^{\mathrm{total}}_A \cdot f_A(C) \\ &\quad + \Delta I^{\mathrm{total}}_A \cdot \Delta f_A \\ &= \Delta I^{\mathrm{total}}_A \cdot \left(1 - f_A(C) + \Delta f_A\right) - I^{\mathrm{total}}_A(C)\cdot \Delta f_A,\end{aligned} \tag{8}$$

and the radiative forcing at doubled CO_2 concentration can finally be expressed as follows:

$$\begin{aligned}\Delta F_{2\times \mathrm{CO}_2} &= \Delta I^{\mathrm{total}}_A \cdot \left(1 - f_A(C) + \Delta f_A\right) - I^{\mathrm{total}}_A(C) \\ &\quad \cdot \Delta f_A - \Delta I_{\mathrm{abs}}.\end{aligned} \tag{9}$$

This CO_2 forcing can directly be derived from radiation transfer calculations (Schwarzschild [30, 31]; Goody and Yung [32]; Salby-2012 [33]; Harde-2013 [18]; Harde-2014 [16]), by which the up- and downwelling fluxes as well as the absorption and emission in the atmosphere are computed.

3. Radiation Transfer Calculations

Since it is obvious that the cloud cover has a strong influence on the up- and downwelling fluxes in the atmosphere and also on the strength of the GH effect, we have performed line-by-line radiation transfer (LBL-RT) calculations under different cloudiness conditions, ground temperatures, and humidity to evaluate the influence of CO_2 on global warming. We also briefly investigate the influence of lineshape effects on RT calculations and their consequences for the ECS.

Here we only present global RT calculation with averaged values for the temperature, water vapor concentration, and an average lapse rate, since separate computations for the tropics mid- and high-latitudes with individual profiles and averaging over the climate zones with an area weighting factor gave almost the same results (see also Harde [16]).

3.1. Clear Sky at Global Mean Temperature. Table 1 shows the results of our LBL calculations under clear sky conditions as a function of the CO_2 concentration, using a ground temperature of $T_E = 289.15\,\mathrm{K} = 16^{\circ}\mathrm{C}$ and a terrestrial intensity of $I_E = 396\,\mathrm{W/m^2}$. These values are consistent with those used by Trenberth et al. [21].

As an average over the three climate zones the water vapor concentration at ground was assumed to be 14,615.3 ppm and decreasing with altitude due to the Clausius-Clapeyron equation (for details see Harde-2014 [16]). These data have been derived from satellite measurements (Vey [34]) and are almost a factor of two larger than those given by the

Table 1: RT-calculations for different CO_2 concentrations at clear sky (I_E = 395.78 W/m^2, T_E = 289.15 K, water vapor at ground: 14615.3 ppm, CH_4: 1.8 ppm, and O_3 varying over the stratosphere with a maximum concentration of 7 ppm).

CO_2 ppm	$I_{\text{total}}^{\text{up}}$ W/m^2	I_A^{up} W/m^2	I_A^{down} W/m^2	I_A^{total} W/m^2	I_{abs} W/m^2	$\mathbf{a}_{\text{LW}}$ %	f_A %
0	290.72	201.03	283.40	484.43	303.09	77.06	58.50
35	272.70	194.92	295.40	490.32	315.00	80.08	60.25
70	269.62	193.96	297.54	491.50	317.13	80.62	60.54
140	266.26	193.22	300.08	493.30	319.75	81.29	60.83
210	264.08	192.86	301.08	493.94	321.57	81.75	60.95
280	262.40	192.64	303.16	495.80	323.02	82.12	61.15
350	261.01	192.50	304.31	496.81	324.27	82.44	61.25
380	260.48	192.45	304.75	497.20	324.76	82.57	61.29
420	259.81	192.41	305.32	497.73	325.38	82.72	61.34
490	258.75	192.36	306.23	498.59	326.40	82.98	61.42
560	257.78	192.34	307.08	499.42	327.34	83.22	61.49
630	256.90	192.35	307.86	500.21	328.23	83.45	61.55
700	256.08	192.37	308.60	500.97	329.07	83.66	61.60
760	255.42	192.40	309.21	501.61	329.76	83.84	61.64
380–760	5.06	0.05	−4.46	−4.41	−5.00	−1.27	−0.35
$\Delta I_A^{\text{up}} - \Delta I_{\text{abs}}$	5.05						

US Standard Atmosphere [35]. But they are in quite good agreement with the Average Global Atmosphere (Ollila [36]), which even specifies values 12% larger than ours. The CH_4 concentration was set to 1.8 ppm and O_3 to vary over the stratosphere with a maximum concentration of 7 ppm at 38 km altitude. The lapse rate and pressure variation with altitude agree with the US Standard Atmosphere.

Our calculations cover a spectral interval from 10 to 2500 cm^{-1}, corresponding to 99.86% of a Planck radiator at T_E, and they include more than 78,000 lines with spectral intensities larger 10^{-24} cm^{-1}/(molecules·cm^{-2}). The spectral resolution for calculations at CO_2 concentrations of 380 and 760 ppm, which are used as reference data, was chosen as 0.07 cm^{-1} (2.2 GHz), and for the vertical direction 228 sublayers were distinguished, whereas the calculations at the other concentrations were performed with half the spectral and vertical resolution.

Comparison of the two last values in column 2 of Table 1 shows that within rounding errors (9) is well confirmed. Looking at the upwelling intensity I_A^{up} of the atmosphere (column 3) we see that this is almost identical at single and doubled CO_2 concentration, while the downwelling part I_A^{down} (column 4) and the total atmospheric radiation I_A^{total} (column 5) both are increasing by more than 4.4 W/m^2. This means that at clear sky conditions most of the additionally absorbed terrestrial radiation at doubled CO_2 (see column 6) is instantaneously directed back to the surface, and only a relatively small contribution of 0.6 W/m^2 is trapped in the atmosphere.

Since in this case the first two terms in (9) almost exactly compensate each other, the forcing under clear sky conditions is in good approximation only determined by the absorption difference. Thus, from the simple radiative forcing model (1) it follows that also the ground temperature variations are almost only determined by this additionally absorbed power.

In general, however, it should be clear that the surface temperature also depends on the emission characteristic of the atmosphere, which changes with the GH gas concentration as well as with the cloud cover and is determined by the first two terms in (9). Only under clear sky they just feed most of the additionally absorbed power back to the surface.

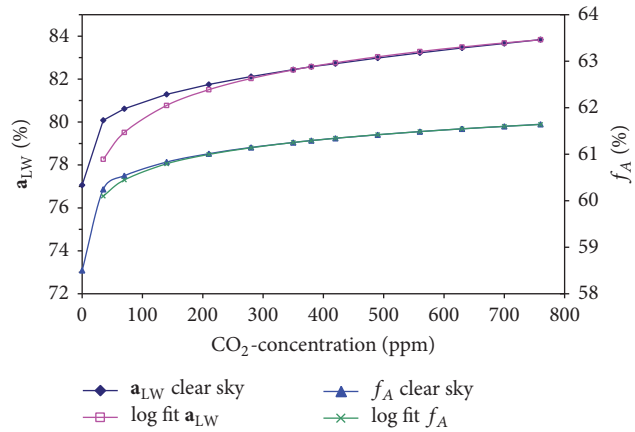

Figure 1: Lw absorptivity $\mathbf{a}_{\text{LW}}$ (black diamonds) and downwelling fraction f_A of emitted atmospheric radiation (blue triangles) at clear sky with respective logarithmic approximations.

In a more advanced model, as this will be discussed later with a radiation and energy balance at TOA and at the surface, including heat fluxes of sensible and latent heat or from neighbouring climate zones, as well as sw and lw absorption losses, even at clear sky conditions the atmospheric emission characteristic is of relevance, which can well be represented by the fraction f_A of the downward emitted radiation.

The relative absorption of terrestrial radiation by the GH gases and its variation with increasing CO_2 concentration are listed in column 7. It is normalized to the incident terrestrial flux and in this way represents the lw absorptivity $\mathbf{a}_{\text{LW}}$ as defined in Harde-2014 [16] (4). This absorptivity is represented in Figure 1 (black diamonds) together with the back-radiated fraction f_A of the atmosphere (blue triangles). At higher concentrations both quantities can well be represented

Table 2: RT-calculations for CO_2 concentrations of 380 and 760 ppm at a surface temperature of 20.3°C (293.45 K) and clear sky (I_E = 420 W/m^2, water vapor at ground: 18,353.2 ppm, CH_4 of 1.8 ppm and O_3 varying over the stratosphere with a maximum concentration of 7 ppm).

CO_2 ppm	I^{up}_{total} W/m^2	I^{up}_A W/m^2	I^{down}_A W/m^2	I^{total}_A W/m^2	I_{abs} W/m^2	$\mathbf{a}_{LW}$ %	f_A %
380	270.22	203.99	334.02	538.01	353.52	84.08	62.08
760	264.76	203.31	338.34	541.65	358.30	85.22	62.46
Δ	5.46	0.68	−4.32	−3.64	−4.78	−1.14	−0.38

by logarithmic graphs (magenta line for $\mathbf{a}_{LW}$, green line for f_A), indicating that due to saturation effects then only the far wings will further contribute to an increasing absorption or emission.

3.2. RT Calculations at Clear Sky and Increased Surface Temperature. Whereas the above calculations reflect a somewhat artificial situation, assuming clear sky and a global mean temperature of 16°C, we know that with declining cloud cover the average surface temperature is significantly climbing up. So, from observations within the International Satellite Cloud Climatology Project (ISCCP) [22] it is found that around the global mean cloud cover of 66% a reducing cloudiness of 1% causes a temperature increase of about 0.06–0.07°C, a tendency which is also confirmed by data of Hartmann [37].

Therefore, to get a better understanding of how such higher temperature modifies the respective fluxes in the atmosphere and especially this affects the CO_2 radiative forcing, we have performed additional calculations for a surface temperature of 20.3°C. At this temperature and a surface emissivity of 100% the terrestrial radiation climbs up to 420 W/m^2. But with the higher temperature also the humidity increases and therefore affects the absorptivity of the GH gases. From the measured water vapor concentrations as well as the temperatures at mid-latitudes and the tropics we deduce at the higher temperature a growth of the vapor concentration of 3,738 ppm with a new total mean concentration near the surface of 18,353 ppm.

Calculations for this higher ground temperature and water vapor concentration are shown in Table 2.

Since for an evaluation of CO_2 with its influence on the radiation budget it is sufficient to concentrate on the fluxes at single and doubled CO_2 concentration, here we only present this reduced data set. Compared to the lower temperature calculations the radiative forcing increases by 0.4 W/m^2, which is mainly due to changes in the upward atmospheric emission with $\Delta I^{up}_A = 0.7$ W/m^2, while the absorption changes with $\Delta I_{abs} = -4.8$ W/m^2 are even getting slightly smaller. Also the downward directed flux change with $\Delta I^{down}_A = -4.3$ W/m^2 and the total atmospheric emission change with $\Delta I^{total}_A = -3.6$ W/m^2 are reducing, although the absolute fluxes and the absorption are considerably larger, caused by the higher temperature and water vapor.

The absorptivity as calculated under these modified conditions is shown in Figure 2 (black diamonds) together with the back-radiated fraction f_A of the atmosphere (blue triangles). At higher CO_2 concentrations both graphs can again well be approximated by logarithmic functions, similar to Figure 1 (magenta line for $\mathbf{a}_{LW}$, green line for f_A), only on slightly shifted scales.

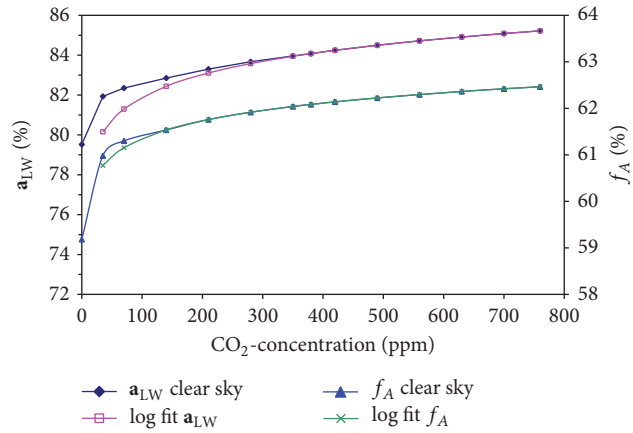

Figure 2: Lw absorptivity $\mathbf{a}_{LW}$ (black diamonds) and downwelling fraction f_A of atmospheric radiation at T_E = 20.3°C and clear sky with respective logarithmic approximations.

3.3. LBL-RT Calculations at Global Mean Cloud Cover. Under regular cloud cover significant changes from clear sky conditions have to be expected for the up- and downwelling fluxes due to the strong shielding effect of clouds not only for sw but also for lw radiation. In our radiation transfer calculations the clouds are considered as a single thinner layer, which absorbs the incident lw radiation from up or down direction with a cloud absorptivity $\mathbf{a}_{LC}$ and which has a transmissivity of $1 - \mathbf{a}_{LC}$, while lw scattering processes at the clouds are here neglected. For the RT calculation only the resulting attenuation of radiation, which passes the layer, is of relevance, and for these calculations it is sufficient to express the total attenuation uniformly only by one parameter, the cloud absorptivity. In addition to the transmitted radiation the clouds are also emitting as a Planckian radiator with an emissivity $\boldsymbol{\varepsilon}_{LC}$ and a temperature determined by the cloud altitude.

The Global Energy and Water Cycle Experiment (GEWEX) Radiation Panel, which compares the available global long-term cloud data products with the ISCCP and consists of 12 satellite measurement teams, specifies the global total cloud amount between 56% and 74% (Stubenrauch et al. [38]), where this relatively wide range is mainly explained by different instrument sensitivity and by retrieval methodology. For our further calculations we assume a global mean cloud cover of $C_C = 66\%$ in agreement

Table 3: RT-calculations for different CO_2 concentrations at mean cloud cover of 66%, a cloud altitude of 5.1 km, and cloud emissivity of 63% (I_E = 396 W/m^2, T_E = 289.15 K = 16.0°C, water vapor at ground of 14,615.3 ppm, CH_4 of 1.8 ppm, and O_3 varying over the stratosphere with a maximum concentration of 7 ppm).

CO_2 ppm	I^{up}_{total} W/m^2	I^{up}_A W/m^2	I^{down}_A W/m^2	I^{total}_A W/m^2	I_{abs} W/m^2	$\mathbf{a}_{LW}$ %	f_A %
0	262.82	210.01	308.62	518.63	342.97	79.34	59.51
35	248.31	202.49	317.89	520.38	349.96	81.09	61.09
70	245.88	201.31	319.57	520.88	351.21	81.40	61.35
140	243.24	200.22	321.55	521.77	352.76	81.78	61.63
210	241.49	199.49	322.83	522.32	353.78	82.05	61.81
280	240.21	199.08	323.89	522.97	354.64	82.29	61.93
350	239.62	199.26	326.14	525.40	355.41	82.49	62.07
380	239.22	199.22	326.49	525.71	355.77	82.57	62.10
420	238.72	199.01	326.93	525.94	356.06	82.67	62.16
490	237.92	198.80	327.64	526.44	356.66	82.83	62.24
560	237.20	198.64	328.29	526.93	357.21	82.97	62.30
630	236.54	198.50	328.90	527.40	357.74	83.10	62.36
700	235.93	198.38	329.47	527.85	358.23	83.21	62.42
760	235.45	198.38	329.94	528.32	358.70	83.31	62.45
Δ	3.77	0.84	−3.45	−2.61	−2.93	−0.74	−0.35
$\Delta I^{up}_A - \Delta I_{abs}$	3.77						

with the ISCCP [22]. The cloud altitude with h_C = 5.1 km and the emissivity with $\boldsymbol{\varepsilon}_{LC}$ = 63% were chosen to almost exactly reproduce the widely accepted radiation and energy budget scheme of Trenberth et al. [21] (hereafter called TFK-scheme) with a total upward flux of I^{up}_{total} = 239.2 W/m^2 and a nonabsorbed outgoing radiation from the surface with $I^{up}_{total} - I^{up}_A$ = 40 W/m^2.

Our RT calculations under otherwise identical conditions as described in Section 3.1 and at a surface temperature T_E = 16°C are listed in Table 3. They show significant changes to the radiation fluxes under clear sky, for example, for I^{down}_A, more than 20 W/m^2 or for I^{total}_A even 28 W/m^2. Also the total absorption, now additionally increased by the clouds, is 31 W/m^2 larger than at clear sky.

But respective differences between single and doubled CO_2 concentrations, which are here of main interest, in general are getting smaller. So, the radiative forcing reduces to $\Delta F_{2\times CO_2}$ = 3.77 W/m^2 and is almost identical with the figure used by the IPCC (Myhre et al. [39]), although here we consider only the instantaneous lw RF at TOA. This forcing is the result of the upwelling atmospheric contribution of ΔI^{up}_A = 0.84 W/m^2 and on the other hand a reduced absorption difference of ΔI_{abs} = −2.93 W/m^2 compared to −5 W/m^2 at clear sky. Also changes in the back-radiation diminish from −4.5 W/m^2 to ΔI^{down}_A = −3.5 W/m^2 and the total emission even from −4.4 W/m^2 to ΔI^{total}_A = −2.6 W/m^2.

Because of this smaller alteration in the atmospheric emission the 1st term in (9) with $\Delta I^{total}_A \cdot (1 - f_A(C) + \Delta f_A)$ now reduces to −0.99 W/m^2, whereas the 2nd term with $-I^{total}_A(C) \cdot \Delta f_A$ = 1.83 W/m^2 dominates. From the total forcing of 3.77 W/m^2 in this case 3.45 W/m^2 goes back to the surface, while 0.32 W/m^2 remains in the atmosphere.

To deduce the lw absorptivity at cloudiness from the radiation transfer calculations, the absorbed intensity listed in column 6 of Table 3, which now reflects the total absorption caused by the GH gases and the clouds, has to be reduced by the cloud fraction. Such correction seems appropriate for a direct comparison of the absorptivity changes caused by the GH gases at clear sky and clouds, and it is necessary for our two-layer climate model, where the cloud absorption is already integrated in the model and represented by respective parameters. Such a correction is done by comparing the absorption, for example, at 380 ppm with and without clouds at the same ground temperature, and reducing column 6 by this difference. Normalizing the corrected absorption to the incident radiation then gives in good approximation the lw absorptivity $\mathbf{a}_{LW}$ of the GH gases in the presence of clouds.

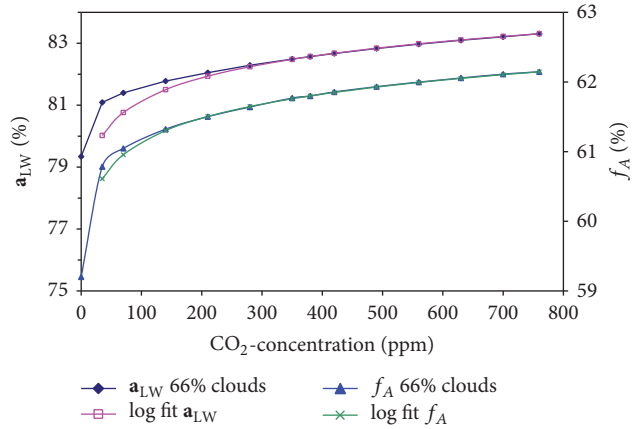

Figure 3: Lw absorptivity $\mathbf{a}_{LW}$ (black diamonds) and downwelling fraction f_A of emitted atmospheric radiation at 66% cloud cover with respective logarithmic approximations.

Figure 3 shows the respective absorptivity $\mathbf{a}_{LW}$ (black diamonds) and the back-radiated fraction f_A (blue triangles) at a cloud cover of 66%. Again both quantities can well be

Table 4: RT-calculations with MRT lineshape for CO_2 concentrations of 380 and 760 ppm at mean cloud cover of 66%, a cloud altitude of 6.0 km, and cloud emissivity of 47.8% (I_E = 396 W/m^2, T_E = 289.15 K = 16.0°C, water vapor at ground of 14,615.3 ppm, CH_4 of 1.8 ppm, and O_3 varying over the stratosphere with a maximum concentration of 7 ppm).

CO_2 ppm	$I_{\text{total}}^{\text{up}}$ W/m^2	I_A^{up} W/m^2	I_A^{down} W/m^2	I_A^{total} W/m^2	I_{abs} W/m^2	$\mathbf{a}_{\text{LW}}$ %	f_A %
380	239.47	199.48	329.41	528.89	355.78	89.77	62.28
760	235.68	198.50	332.59	531.09	358.60	90.48	62.62
Δ	3.79	0.98	−3.18	−2.20	−2.82	−0.71	−0.34

represented by logarithmic graphs (magenta line for $\mathbf{a}_{\text{LW}}$, green line for f_A). While f_A slightly increases by 0.8%, Δf_A remains constant. However, the absorptivity changes almost decline by a factor of two to −0.74% at doubled CO_2 concentration.

Simulations at higher cloud altitudes under otherwise same constrains give a reduced upwelling flux $I_{\text{total}}^{\text{up}}$ and a further diminishing radiative forcing $\Delta F_{2\times CO_2}$.

3.4. RT Calculations with MRT Lineshape. While the preceding calculations are based on the standard molecular collision theory, considering collisional broadening of spectral transitions, which are characterized by a Lorentzian lineshape or at higher altitudes also by a Voigt profile, we have also performed extensive calculations using a more sophisticated lineshape as given by the molecular response theory (MRT) (Harde et al. [40–44]). This theory represents a generalization and unification of the classical collision theories of Lorentz and on the other hand of van Vleck and Weisskopf, considering thermalization of molecules during a collision, which in its limit is determined by the reciprocal of the molecular transition frequency and controlled by Heisenberg's uncertainty principle (Harde & Grischkowsky [44]). The specialty applying MRT is that it not only describes the near resonance absorption and emission behavior as already adequately characterized by a Lorentzian, but also reflects the far wing response, which is mainly caused by the ultrafast time response of molecules to an external electric field during collisions. So, the MRT lineshapes already represent very well the continuum water vapor absorption extending up to 1200 cm^{-1} and caused by the low frequency water vapor absorption band around 200 cm^{-1} (see Burch & Gryvnak [45]; Roberts et al. [46]).

This continuum water vapor background together with the far wing contributions of the other molecules significantly modifies the absolute up- and downwelling fluxes. Therefore, to further satisfy the radiation and energy balance of the TFK-scheme, in the radiation transfer calculations the cloud altitude has to be increased to 6 km and the cloud absorptivity = emissivity reduced to 47.8%.

The results of such a calculation at a mean cloud cover of 66% and at otherwise same conditions as described in Section 3.3 is shown in Table 4. To compare the alterations caused by doubling the CO_2 concentration it is again sufficient only to display the calculations for 380 and 760 ppm CO_2. It is interesting to see that the more sophisticated lineshape and the continuum background absorption almost have no influence on $\Delta F_{2\times CO_2}$, the RF at doubled CO_2, which agrees within better than 1% with the simpler calculations shown in Table 3, neglecting the continuum absorption and using a Lorentzian lineshape. Also changes in the other fluxes at doubled CO_2 concentration are consistent within 0.1 W/m^2; only the back-radiation changes to $\Delta I_A^{\text{down}} = -3.18$ W/m^2 and is about 0.3 W/m^2 smaller; thus, the power left in the atmosphere increases by this amount.

For this insensitivity to a different collision and lineshape theory we see three main reasons: first, because of the larger absolute flux variations, caused by the different wing absorption and WV continuum, the outgoing fluxes were recalibrated to the TFK-scheme via cloud altitude and absorptivity to ensure comparable absolute fluxes in agreement with the observations. Second, we only consider flux differences at single and doubled CO_2 concentration for the same shape, so that discrepancies to another shape are not directly observed and smaller absolute variations with the CO_2 concentration are to some extent cancel out. Third, the interference of the CO_2 spectrum with strong water vapor lines and the underlying WV continuum further attenuates any CO_2 lineshape effects.

So, calculations based on the classical collision theory obviously reproduce quite reliable data of any radiation changes in the atmosphere. Since the far wings of the CO_2 lines are found to decay more rapidly than a Lorentzian and thus should contribute less to the total absorption (see, e.g., Edwards and Strow [47]), such calculations even simulate slightly worse conditions and result in a more conservative assessment of global warming by CO_2. For actual CO_2 lineshape studies see also Happer [48], and for RT calculations including CO_2 line mixing see Mlynczak et al. [49], and Ozak et al. [50].

3.5. RT Calculations for Total Cloud Cover. With a further increasing cloud cover and thus a stronger shielding of the sw radiation also the surface temperature further drops, and owing to the ISCCP observations at 100% cloudiness then a reduced temperature of approximately 2.2°C compared to mean cloudiness is expected.

Respective radiation transfer calculations at 100% cloud cover, a surface temperature of 13.8°C with a terrestrial intensity of 384 W/m^2, and a further reduced water vapor concentration at ground of 12,703 ppm, otherwise using the same conditions as in Section 3.3, are shown in Table 5. The total outgoing radiation $I_{\text{total}}^{\text{up}}$ drops by 15.4 W/m^2 and the total atmospheric emission I_A^{total} by 6.6 W/m^2 compared

Table 5: RT-calculations for different CO_2 concentrations at 100% cloudiness, a cloud altitude of 5.1 km, and cloud emissivity of 63% (I_E = 384 W/m^2, T_E = 286.95 K = 13.8°C, water vapor: 12,702.9 ppm, CH_4: 1.8 ppm, and O_3 varying over the stratosphere with a maximum concentration of 7 ppm).

CO_2 ppm	$I_{\text{total}}^{\text{up}}$ W/m^2	I_A^{up} W/m^2	I_A^{down} W/m^2	I_A^{total} W/m^2	I_{abs} W/m^2	$\mathbf{a}_{\text{LW}}$ %	f_A %
380	223.80	197.75	321.34	519.09	357.86	81.55	61.90
760	220.84	196.72	324.27	520.99	359.79	82.05	62.24
Δ	2.96	1.03	−2.93	−1.90	−1.93	−0.50	−0.34

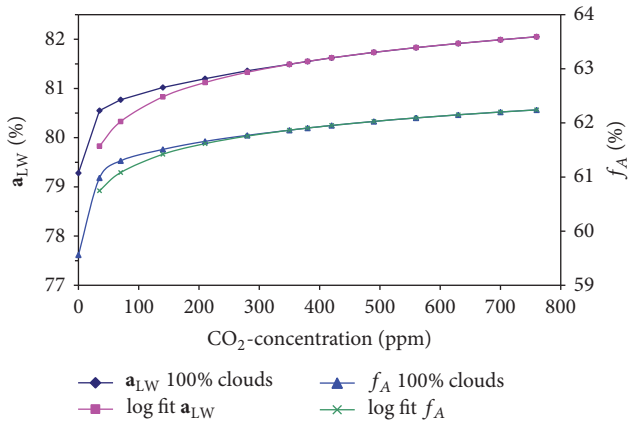

Figure 4: Lw absorptivity $\mathbf{a}_{\text{LW}}$ (black diamonds) and downwelling fraction f_A (blue triangles) of emitted atmospheric radiation at 100% cloudiness and a ground temperature of 13.8°C with respective logarithmic approximations.

to a cloud cover of 66%. Nevertheless, the forcing due to doubled CO_2 reduces to $\Delta F_{2\times CO_2}$ = 3.0 W/m^2, consisting of a slightly increasing contribution ΔI_A^{up} = 1.0 W/m^2 and a decreasing absorption ΔI_{abs} = −1.9 W/m^2. Also the absolute downwelling radiation I_A^{down} further decreases by 5.2 W/m^2, and its alteration at doubled CO_2 concentration reduces to −2.9 W/m^2, so almost nothing remains in the atmosphere.

The absorptivity $\mathbf{a}_{\text{LW}}$ as listed in column 7 is again found by comparing the absorption at 380 ppm with clouds (357.86 W/m^2) and without clouds (313.57 W/m^2), reducing column 6 by this difference and then normalizing the corrected absorption to the incident radiation. $\mathbf{a}_{\text{LW}}$ is shown together with the parameter f_A in Figure 4. Both graphs can again well be represented by logarithmic plots.

The changes in absorptivity from single to doubled CO_2 with $\Delta\mathbf{a}_{\text{LW}}$ = −0.5% further decline compared to 66% cloudiness or clear sky, and also Δf_A is slightly reducing to −0.34%.

So, from these calculations it is clear that the up- and downwelling fluxes and also the absorption in the atmosphere are significantly varying with the cloud clover and, therefore, they will also significantly influence the global mean surface temperature. But it can also well be recognized, that changes with the CO_2 concentration by trend get smaller with increasing cloudiness.

4. Assessment of CO_2 Global Warming

Different to general circulation models, which try to predict local climate variations over some time period and, therefore, have to solve complex coupled nonlinear differential equations with a large number of parameters, making these calculations extremely time consuming and even unstable, for computing the equilibrium climate sensitivity C_S it is sufficient to rely on a much simpler model, which calculates an equilibrium energy and radiation balance and averages over larger local variations.

But independent of the model's complexity, almost all known models are based on the simple relation given by (1) that the ground temperature is scaling proportional with the radiative forcing of an external perturbation. Any feedback processes, for example, by water vapor, albedo, the lapse rate, or clouds, are generally included in this equation as an additional prefactor $(1 - \text{f} \cdot \lambda_S)^{-1}$ in the following form:

$$\Delta T_E = \frac{\lambda_S}{1 - \text{f} \cdot \lambda_S} \cdot \Delta F, \tag{10}$$

where f is the feedback parameter, by which all linear and nonlinear responses of EASy to a changing surface temperature are represented (see also Lindzen & Choi [28], only using different symbols).

Thus, the simplest way to assess C_S is to directly apply (10) with the known feedback and radiative forcing. Often, however, this calculus method suffers from the fact

(i) that the Planck sensitivity λ_S has to be adapted from other models;

(ii) that it is difficult to distinguish between different forcings with different feedbacks;

(iii) that this method only considers a radiation balance at the tropopause or TOA, but not an additional radiation and energy balance at the surface;

(iv) that it does not consider the feedback of the atmosphere to the surface and vice versa, caused by radiation changes as well as changes of sensible and latent heat;

(v) that some feedback processes and their evaluation are not really retraceable from other sources;

(vi) and that for simplicity reasons often sw feedback effects are completely neglected.

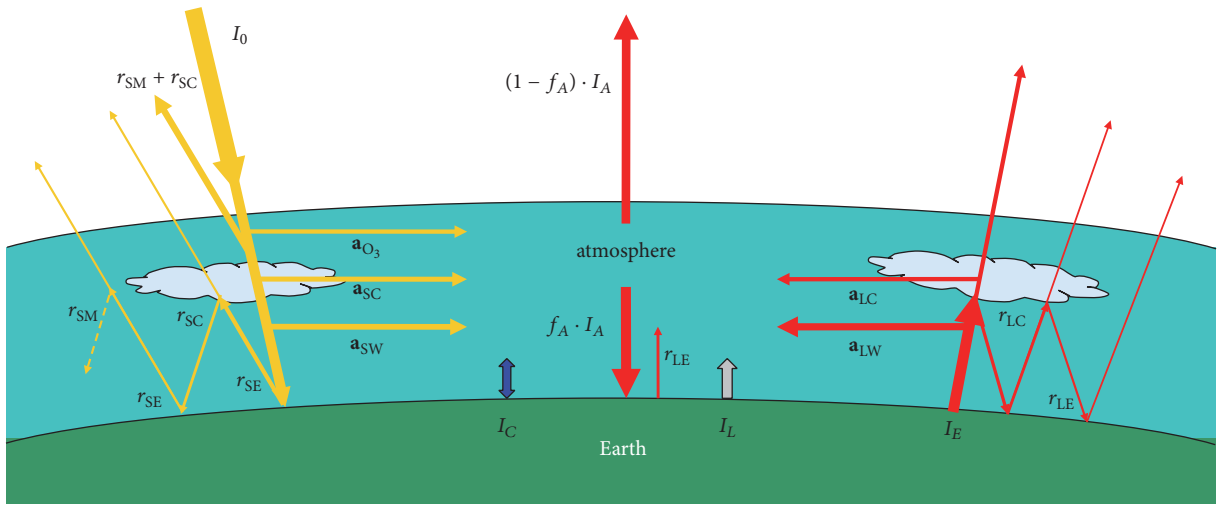

FIGURE 5: Two-layer climate model for the Earth-atmosphere system with the main parameters.

Therefore, here we use our own advanced two-layer climate model, which is free from these deficits and which then can be compared with the IPCC accounting scheme or other methods. In addition, we investigate the effect and the size of the slightly changing reradiation of the atmosphere with increasing CO_2 concentration as represented by the back-radiated fraction f_A.

4.1. Model Adaptation to Satellite Measurements. Our two-layer climate model is especially appropriate to calculate the influence of the increasing CO_2 concentrations on global warming as well as the impact of solar variations on the climate. The model describes the atmosphere and the ground as two layers acting simultaneously as absorbers and Planck radiators. It includes additional heat transfer between these layers due to convection and evaporation, and it considers cloud effects for the sw and lw radiation as well as all relevant feedback effects like water vapor, lapse rate, albedo, cloud cover, convection, and evaporation. At equilibrium both the atmosphere and the ground release as much power as they absorb from the Sun and the neighbouring layer. An external perturbation, caused by variations of the solar activity or the GH gases, then forces the system to come to a new equilibrium with new temperature distributions of EASy. Figure 5 shows the main features of the two-layer climate model with its relevant parameters.

Different to other schemes, in our model the key parameters are not the radiative forcing, but the sw and lw absorptivities $\mathbf{a}_{SW}$ and $\mathbf{a}_{LW}$ as well as the back-radiated fraction of the atmosphere f_A, all of which are varying with the CO_2 concentration (see Figures 1–4). Whereas the sw absorptivity can well be adopted from our previous calculations (Harde-2014 [16]), for the actual simulations we use the new and more advanced radiation transfer calculations, presented in Section 3, which clearly distinguish between clear sky and cloudy conditions. All other parameters like the cloud and sw ozone absorptivities, the scattering coefficients at clouds and the atmosphere, and the Earth's reflectivities were adapted in such a way that all radiation and heat fluxes almost exactly reproduce the widely accepted TFK-scheme (see also Harde-2014 [16], Fig. 10), which essentially relies on data from satellite measurements within the ERBE and CERES program [51–55]. This adaptation yields a calibration of our model to the observed up- and downwelling fluxes under standard conditions in the atmosphere and for constant heat fluxes between the surface and atmosphere. All relevant parameters are listed in Table 6.

Compared to our previous simulations (Harde-2014 [16]) some of these parameters had slightly to be modified to further reproduce the TFK-scheme, this as a consequence of the changing fluxes and absorptivities with the ground temperature at clear sky or cloudiness. Particularly to reproduce the measured temperature variations with the cloud cover, the parameters r_{SM} and r_{SC} had to be adjusted to satisfy the TFK, as well as the ISCCP observations. In this sense our model is similar to the energy budget ESC estimates, which provide an independent observationally based constraint of this important parameter (see Lewis & Crok [17], Forster & Gregory [27], and Lindzen & Choi [28]).

For the temperature response of EASy and, thus, the calibration of the model we relate to the temperature anomaly data of the Hadley Centre and Climate Research Unit (HadCRUT3) as a function of the monthly global cloud cover data of the ISCCP (scatter diagram of O. Humlum, http://www.climate4you.com/ [22]) with a response of −0.065°C/%, while a reverse scatter plot for the same ISCCP data over the Berkley Earth Surface Temperature (BEST) leads to a much stronger temperature variation with cloud cover of about −0.3°C/%. Consequences for a thermally induced cloud cover feedback will be discussed in Section 4.3.6.

Our climate model also contains a parameter for the lw scattering at clouds (r_{LC}) with the ability of multiple reflections between clouds and the surface. Since this quantity has no meaning in an RT calculation, considering only a one way propagation of radiation, the respective adaptation of the

Table 6: Parameter set at mean global cloud cover and mean temperature to reproduce the TFK data.

Parameter	Symbol	Unit	Value
averaged solar flux	I_0	W/m^2	341.3
cloud cover	C_C	%	66.0
sw molec. scattering coef.	r_{SM}	%	13.2
sw cloud scattering coef.	r_{SC}	%	18.14
sw Earth reflectivity	r_{SE}	%	17.0
sw ozone absorptivity	$\mathbf{a}_{O_3}$	%	8.0
sw cloud absorptivity	$\mathbf{a}_{SC}$	%	12.15
sw H_2O-CO_2-CH_4 absorptivity	$\mathbf{a}_{SW}$	%	14.51
lw Earth's reflectivity	r_{LE}	%	0.0
lw cloud scattering coef.	r_{LC}	%	20.9
lw cloud absorptivity	$\mathbf{a}_{LC}$	%	54.1
lw H_2O-CO_2-CH_4-O_3 absorptivity	$\mathbf{a}_{LW}$	%	82.58
Earth's emissivity	ε_E	%	100.0
atmospheric emissivity	ε_A	%	87.5
back-radiated fraction	f_A	%	61.8
sensible heat flux	I_C	W/m^2	17.0
latent heat flux	I_L	W/m^2	80.0

total upward flux and direct flux from the surface had to be fitted in the RT calculations via the cloud absorptivity $\mathbf{a}_{LC}$, which, therefore, differs from the absorptivity used in the 2LCM.

The up- and downward fluxes as calculated by the two-layer climate model are compiled in Table 7 and show the excellent agreement with the TFK data. The smaller deviations mainly result from the fact that the fluxes in the TFK-scheme are not completely balancing in up- and downward direction but contribute to a net surface absorption of 0.9 W/m^2, while our calculations are valid for steady state conditions with an exact balance between the absorbed solar radiation and the OLR.

It should also be noticed that the direct flux from the surface to TOA with 40 W/m^2 can only be realized with a relatively high lw cloud scattering and medium cloud absorption. These parameters mainly determine the reference temperature T_R and lw fluxes but have negligible influence on calculations of the ECS. So, for example, for $r_{LC} = 0$ and $\mathbf{a}_{LC} = 77\%$, for which the direct flux declines by 6 W/m^2, while the indirect flux increases by the same amount, the climate sensitivity stays the same.

Since the objective of our investigations here is to evaluate the influence of CO_2 on global warming, the parameters in Table 6 and the fluxes in Table 7 primarily define a working point for further considerations; in particular they determine the reference temperature $T_R = 16^\circ$C of the Earth's surface at a CO_2 concentration of 380 ppm. Only deviations from this reference, caused by a changing CO_2 concentration and the different feedback processes, are of further interest, not so much absolute temperature levels.

Table 7: Comparison of calculated fluxes under regular atmospheric conditions with the TFK data.

Flux (W/m^2)	This model	TFK data
sw: incoming solar radiation	341.3	341.3
backscattered from molecules	14.1	
backscattered from clouds	65.0	
together backscattered	79.0	79
reflected at Earth's surface	22.9	23
total reflected solar radiation	101.9	101.9
absorbed by O_3,	27.3	
clouds,	19.1	
water vapor, CO_2, CH_4	31.6	
total absorption of atmosphere	78.0	78.0
absorption in surface	161.3	161
lw: surface radiation	396.3	396
absorbed by GH-gases	327.3	
absorbed by clouds	19.5	
backscattered by clouds	9.5	
absorb. & scat. surface radiation	356.3	356
sensible heat	17.0	17
latent heat	80.0	80
total absorption in atmosph.	521.8	
outgoing radiation fr. atmosph.	199.3	199
outgoing directly from surface	40.0	40
total outgoing radiation	239.4	238.5
back-radiation	331.9	333
net emission of surface	64.4	
total outgoing radiation at TOA	341.3	340.4

4.2. Direct Influence of CO_2. First we consider the simplest case, neglecting any feedback processes and looking only to the direct influence of CO_2 on global warming. With the sw and lw absorptivities as well as the back-radiated fraction integrated in the climate model, the Earth's surface temperature and the lower tropospheric temperature are simulated as a function of the CO_2concentration. For details, how these temperatures are calculated by the 2LCM and how they are defined, see Harde-2014 [16], Subsection 4.4.

For the case of clear sky ($C_C = 0$) this is shown in Figure 6(a), where the red graph indicates Earth's temperature T_E at the surface and the blue graph the lower tropospheric temperature T_A as derived from the Stefan-Boltzmann relation when inserting the back-radiated power. The increase of T_E at doubled CO_2 concentration (from 380 to 760 ppm) defines the CO_2 climate sensitivity as a measure for the response of EASy on a changing CO_2 concentration. At clear sky conditions and without feedback effects this climate sensitivity is found as $C_S = 1.79^\circ$C, which is significantly

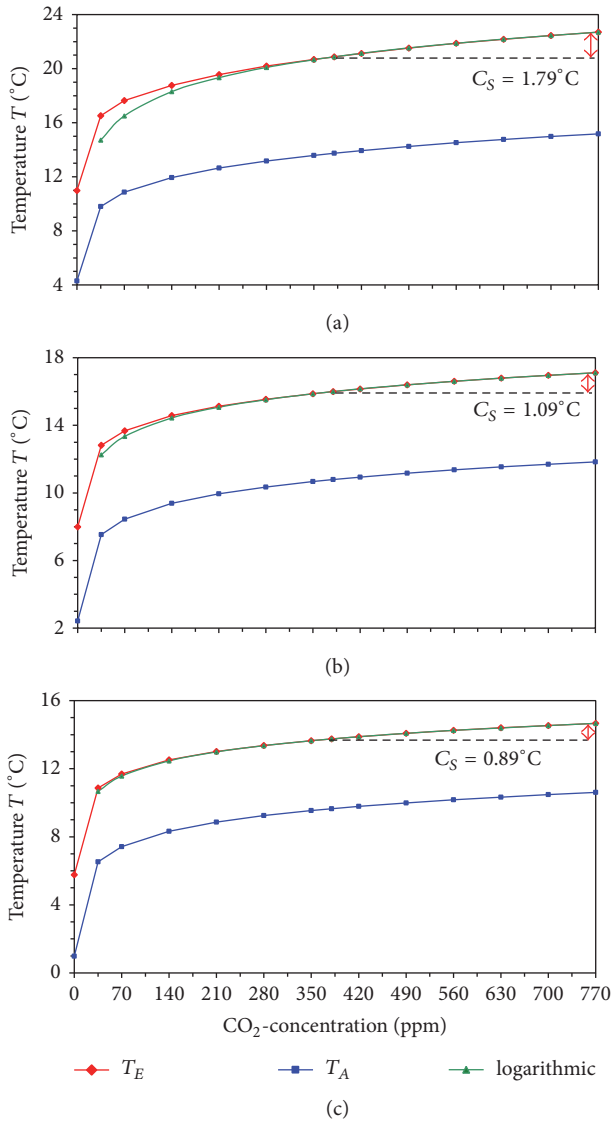

FIGURE 6: Calculated Earth temperature T_E (red) and lower tropospheric temperature T_A (blue) as a function of the CO_2 concentration under (a) clear sky, (b) 66% cloud cover, and (c) total cloudiness. Logarithmic approximations are plotted as green lines.

larger than our previously published value of 1.1°C (Harde-2014 [16]).

The reason for this discrepancy is twofold. So, the new RT calculations (see Section 3.2) were performed for a ground temperature at clear sky of 20.3°C, which increases the lw absorptivity due to water vapor and, thus, lifts the climate sensitivity by about 0.4°C. Another contribution of 0.3°C is initiated by the back-radiation, which slightly changes via f_A with the CO_2 concentration (Figure 2). Although at clear sky the radiative forcing $\Delta F_{2\times CO_2}$ is almost only determined by the absorption losses in the atmosphere (see Table 2), the small variation Δf_A of less than 0.4%, multiplied with the total atmospheric emission I_A^{total}, causes this additional increase in our model (see second term in (9)).

A higher cloudiness not only reduces the average surface temperature but also diminishes the climate sensitivity. This can be seen from Figures 6(b) and 6(c), showing the surface and atmospheric temperature at the mean cloud cover of 66% and 100% as a function of the CO_2 concentration. At 66% cloudiness the climate sensitivity declines to C_S = 1.09°C, while at 100% it even reduces to 0.89°C.

The green graphs in Figure 6 represent logarithmic fits, indicating that due to saturation effects and only far wing absorption at higher CO_2 concentrations the surface temperature can well be approximated by a logarithmic function of the following form:

$$T_E(C) = T_E(C_0) + \lambda_S \cdot \alpha \cdot \ln\left(\frac{C}{C_0}\right) = T_E(C_0) + \lambda_S \cdot \Delta F_{2\times CO_2} \frac{\ln(C/C_0)}{\ln 2}, \quad (11)$$

where $T_E(C_0)$ is the temperature at a CO_2 concentration C_0 = 380 ppm, λ_S is the Planck sensitivity as it results from our two-layer climate model, and α is defined as $\alpha = \Delta F_{2\times CO_2}/\ln 2$ (see also Myhre et al. [39]).

For the special case $C = 2 \cdot C_0$, (11) merges into (1), and we see that either λ_S can be derived from a logarithmic fit to the temperature data or from the climate sensitivity using (1). Table 8 summarizes the related quantities, which characterize the influence of CO_2 on global warming under different cloud situations, but neglecting feedback processes. From these data we can assert that the Planck sensitivity, as deduced from our two-layer model, agrees within 8% with the model mean of the Coupled Model Intercomparison Project Phase 5 (CMIP5) AOGCMs (AR5-WG1-Tab.9.5) and is slightly varying with the cloud cover. The same holds for the reciprocal value, the Planck feedback.

In this context it should be emphasized that the climate sensitivities from our model were derived with the sw absorptivity changes included, while $\Delta F_{2\times CO_2}$ in (11) only represents the lw RF at TOA, different to AR5.

While the declining temperatures are a direct consequence of the dominating shielding effect for solar radiation, the smaller sensitivities are the result of the increasing influence of the lw cloud absorption and backscattering, by which the importance of the GH-gases is more and more repelled.

We also see that in comparison to the surface the lower atmosphere is responding less sensitively to the CO_2 changes. This may be explained due to the changing radiation and energy balance between the surface and atmosphere with an increasing up- and downward emission of the atmosphere. But the difference between the two curves is more and more reducing at higher cloudiness.

4.3. Feedback Processes. Many climate models agree within acceptable limits in their prediction for the CO_2 climate sensitivity, as long as feedback effects are excluded. But big discrepancies can be observed, when different feedback processes and also climate drivers are included. One reason may be the complexity of these effects, from which their interrelated actions and their mutual interference are not

Table 8: Compilation of some figures at clear sky, global mean cloud cover, and total cloudiness.

Quantity/parameter	Symbol	Unit	Value		
cloud cover	C_C	%	0	66	100
surface temperature	T_E	°C	20.3	16.0	13.8
climate sensitivity	C_S	°C	1.79	1.09	0.89
CO_2 radiative forcing	$\Delta F_{2\times CO_2}$	W/m^2	5.46	3.77	2.96
Planck sensit. this model	λ_S	W^{-1} m^2 °C	0.33	0.29	0.30
Planck feedb. this model	$-1/\lambda_S$	W/m^2/°C	−3.05	−3.47	−3.31
Planck feedback, AR5	$-1/\lambda_S$	W/m^2/°C		−3.20	

really known. Another reason can also be a wrong or undifferentiated assignment of the feedbacks to a specific climate driver, or the simple neglect of an effect.

In this subsection we first consider the influence and size of the well known feedback processes caused by water vapor, the lapse rate, or albedo. Further we investigate the additional effects of convection, evaporation, and cloud cover feedback, which in this form are not discussed and the first ones are even not mentioned in AR5.

4.3.1. Water Vapor Feedback. Water vapor (WV) is by far the largest contributor to the natural GH effect and, therefore, plays an essential role in Earth's climate (AR5-WG1-Chap.8.1). Since its amount in the atmosphere is only controlled by the air temperature, rather than by emissions, scientists consider it as a feedback agent, rather than a forcing to climate change.

In AR5 we read as follows: "the contribution of water vapor to the natural greenhouse effect relative to that of CO_2 depends on the accounting method, but can be considered to be approximately two to three times greater." With respect to their relative concentrations in the atmosphere this proportion appears very small, as an amplifier for the basic climate sensitivity; however, it is quite significant and has to be investigated in more detail.

Indeed, different methods can be applied to estimate this ratio, and their results deviate significantly, depending on what is made responsible for the GH effect and its definition. So, similar to the procedure used to determine the RF at doubled CO_2, one way is first to calculate the total upwelling intensity without WV, I^{up}_{total} (no WV), minus the intensity with all GH gases in the atmosphere I^{up}_{total} (all). At global mean cloud cover and with MRT lineshapes (see also Table 4) this gives a difference I^{up}_{total} (no WV) − I^{up}_{total} (all) = 298.5 − 239.5 = 59 W/m^2. Next one has to calculate the difference between the intensities without CO_2 and with all gases yielding I^{up}_{total} (no CO_2) − I^{up}_{total} (all) = 263.1 − 239.5 = 23.6 W/m^2. Comparison of these differences gives a ratio of 59/23.6 = 2.5 in good agreement with AR5. However, this method essentially characterizes the efficiencies of these gases to block the OLR to space, and thus primarily reflects the radiation balance at TOA, but not so much at the surface.

Therefore, another way of accounting is to consider the differences of the downwelling intensities, which at cloudiness result in I^{down}_A (all) − I^{down}_A (no WV) = 329.4 − 139.3 = 190.1 W/m^2 and I^{down}_A (all) − I^{down}_A (no CO_2) = 329.4 − 315.0 = 14.4 W/m^2 with a ratio 190.1/14.4 = 13.2. This method is particularly sensitive to the contributions of WV or CO_2 at the surface and shows the dominating influence of WV in the lower troposphere, which in this accounting scheme contributes about 60% to the GH effect, while CO_2 is donating not more than 4% and thus relativizes the importance of CO_2 as a dangerous climate driver in the atmosphere. An even slightly larger ratio of WV to CO_2 to the GH effect of about 14 can be found, when calculating the back-radiation under clear sky conditions. A similar result is found considering only the absorption of the terrestrial radiation, first for all gases and then without one of the components, yielding a weighting ratio of 15.

With respect to feedback processes these numbers look quite dramatic. But the contribution of a gas or vapor to the GH effect does not automatically determine its influence as a feedback agent. Therefore, this has to be considered more extensively.

Due to the Clausius-Clapeyron equation the WV content is rapidly increasing with rising temperatures. So, from GPS-measurements (Vey [34]) of the water content in different climate zones we can derive the average WV concentration in a zone (see Harde-2014 [16], Fig. 1), and with the temperature differences between these zones we then estimate that with every extra degree of air temperature the atmosphere retains 5.9% more water vapor. Therefore, also the WV absorption is further increasing and generally contributes to a positive feedback in the total budget. In the literature this feedback is designated as the most serious effect with dramatic amplification values. So in AR5-WG1-Chap.8 we can read "*although CO_2 is the main anthropogenic control knob on climate, water vapor is a strong and fast feedback that amplifies any initial forcing by a typical factor between two and three.*"

Our own investigations, however, show a less dramatic influence of water vapor. One aspect is that, similar to CO_2, also the water lines are already strongly saturating over wider spectral regions. Therefore, with increasing vapor concentration only the far wings of these lines and weak absorption bands can further contribute to an additional absorption, which roughly logarithmically increases with the vapor concentration.

Another aspect is that always both sw and lw absorption have to be considered. Whereas the lw outgoing radiation is more efficiently blocked and thus contributes to a positive

Table 9: sw absorptivity $\mathbf{a}_{SW}$, total lw absorptivity $\mathbf{a}_T$, and back-radiated fraction f_A as a function of the surface temperature and water vapor concentration in three climate zones.

Climate zone	T_E °C	C_{WV} ppm	$\mathbf{a}_{SW}$ %	$\mathbf{a}_T$ %	f_A %
High-lat.	−7	2,359	12.5	81.5	59.2
Mid-lat.	8	7,253	13.4	85.5	61.0
Tropics	26	22,900	15.2	90.8	62.9

feedback, the sw radiation is also more strongly absorbed in the atmosphere, and less of it reaches the surface, which supplies a negative feedback contribution.

Table 9 shows the results of our calculations for the sw absorptivity $\mathbf{a}_{SW}$, the total lw absorptivity $\mathbf{a}_T$ (including cloud absorption), and the back-radiated fraction f_A, which, different to our computations in Section 3, for these feedback studies were calculated at a fixed CO_2 concentration of 380 ppm, but for three climate zones with different surface temperatures and, thus, also different WV concentrations C_{WV}. While $\mathbf{a}_{SW}$ was taken over from Harde [16], the lw absorptivity and f_A were derived under conditions as described in Section 3.4, assuming a cloud cover of 66%, a cloud altitude of 6 km, and a cloud emissivity of 48% and using MRT lineshapes, which already include the WV continuum. We have used the same global mean cloud cover and height over all zones. For typical expected cloud variations over the zones and comparing this with the case of clear sky we estimate that this simplification results in an error of less than 5%. Variations of the cloud cover with temperature and their feedback effects are discussed in Section 4.3.6. For the actual feedback analyses it is sufficient and even preferential only to consider the total lw absorptivity, which we designate as $\mathbf{a}_T$ and which consists of the absorption by GH gases as well as by clouds.

Figure 7 displays the three key parameters $\mathbf{a}_{SW}$, $\mathbf{a}_T$, and f_A as a function of the surface temperature. The red and the blue line as fits to the calculations directly reflect the temperature dependence of the absorptivities, which at constant gas concentrations would have slightly dropped with increasing temperature but due to the dominating growth of the WV concentration results in a net increase. The linear incline is the result of an exponential growth of the WV concentration with temperature due to Clausius-Clapeyron and on the other hand a logarithmic growth of the absorptivities with the vapor concentration due to saturation effects.

The sw and lw absorptivity changes can well be represented by straight lines with the slopes

$$\frac{d\mathbf{a}_{SW}}{dT_E} = 0.10\%/^{\circ}\mathrm{C}, \tag{12}$$

$$\frac{d\mathbf{a}_T}{dT_E} = 0.28\%/^{\circ}\mathrm{C}. \tag{13}$$

For clear sky calculations we further use the value $d\mathbf{a}_{LW}/dT_E = 0.38\%/^{\circ}\mathrm{C}$ (Harde [16], (80)).

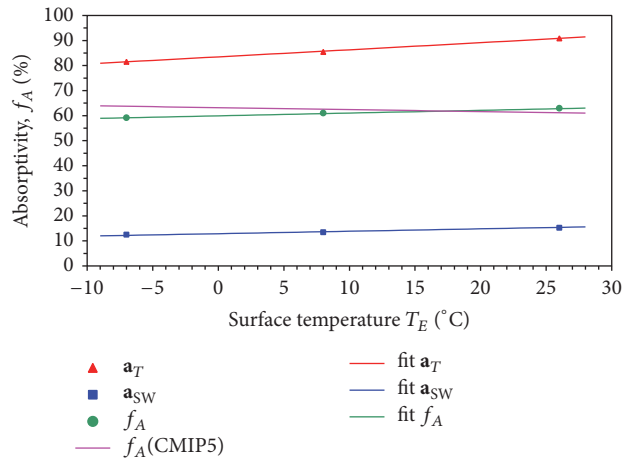

Figure 7: sw absorptivity (blue squares and fit), total lw absorptivity (red triangles and fit) and back-radiated fraction (green circles and fit) for high-latitudes, mid-latitudes, and the tropics. Additionally shown is the predicted back-radiated fraction due to CMIP5 as magenta line.

The back-radiated fraction f_A (green circles in Figure 7) as a function of the surface temperature can also well be represented by a straight line with the slope

$$\frac{df_A}{dT_E} = 0.11\%/^{\circ}\mathrm{C}. \tag{14}$$

While our calculations in Section 3 describe the variations of f_A with the CO_2 concentration and also with cloudiness (see Figures 1–4), this graph displays the additional response of f_A on the temperature and the humidity changes. This response is a typical feedback process, which modifies the up- and downwelling fluxes with the surface temperature and, thus, influences the total radiation and energy balance of EASy. Although the main part of this feedback can be traced back to the increasing WV concentration with temperature, another contribution can be induced by changes of the vertical temperature distribution over the atmosphere and, thus, by changes in the lapse rate. Since it is not advisable to further split these contributions, the temperature dependence of f_A as a whole will be considered in more detail in the next subsection as lapse rate feedback.

Now, taking advantage of (12) and (13) the WV feedback can directly be integrated in our model. This is realized by an iterative procedure, which has been explained in more detail elsewhere (Harde-2014 [16], Section 4, pp. 26-27). In a first step the temperature deviation from the reference temperature T_R, caused by a deviation of CO_2 from the reference concentration (here 380 ppm), is calculated. This T-offset is used to compute with (12) and (13) the corrections in the absorptivities. With the new values again corrected temperatures are determined, which give new absorption corrections. This is repeated, until the temperatures show self-consistency.

The result of such a calculation with WV feedback is illustrated in Figure 8, showing the temperature increase of

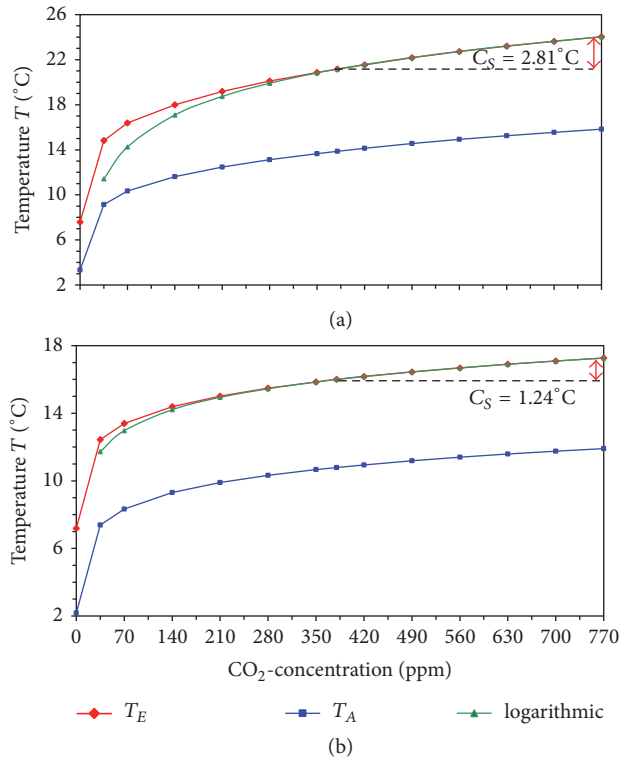

FIGURE 8: Calculated Earth temperature T_E (red) and lower tropospheric temperature T_A (blue) as a function of the CO_2 concentration under (a) clear sky and (b) 66% cloud cover, both with water vapor feedback. Logarithmic approximations are plotted as green lines.

T_E and T_A as a function of the CO_2 concentration. At clear sky (Figure 8(a)) the climate sensitivity rises up from $C_S = 1.79^\circ$C to 2.81°C, which results in an amplification factor due to the WV feedback of 1.57, or in terms of the feedback parameter (see (9)) gives $f_{WV} = 1.10\,W/m^2/^\circ C$. At global mean cloud cover (Figure 8(b)), however, C_S only increases from 1.09°C to 1.24°C, corresponding to an amplification of 1.14 or to a feedback of $f_{WV} = 0.43\,W/m^2/^\circ C$.

Compared to AR5-WG1-Tab.9.5, where the WV feedback is specified as a model mean of $f_{WV} = 1.6 \pm 0.3\,W/m^2/^\circ C$ (corresponding to an amplification factor of two), this is a significant discrepancy, even to our clear sky result.

The reasons for this discrepancy are manifold. So, as already mentioned, our calculations also consider the sw absorptivity, which causes a negative feedback, while this is not clear for the feedbacks specified in AR5. The main differences, however, go back to the procedures applied to determine the changes of $\mathbf{a}_{LW}$ or $\mathbf{a}_T$ with temperature, independent of any variations in f_A. This can best be retraced considering the most important contributions, which are responsible for these changes.

Quite generally we can distinguish two effects and write

$$d\mathbf{a}_{LW,T} = \frac{\partial \mathbf{a}_{LW,T}}{\partial C_{WV}} \frac{\partial C_{WV}}{\partial T_E} dT_E + \frac{\partial \mathbf{a}_{LW,T}}{\partial \sigma_{LW}} \frac{\partial \sigma_{LW}}{\partial T_E} dT_E, \quad (15)$$

with $\partial \mathbf{a}_{LW,T}/\partial C_{WV}$ as the partial derivative describing the lw (total) absorptivity changes as a function of the water vapor concentration C_{WV}, $\partial C_{WV}/\partial T_E$ as the changes of C_{WV} with the surface temperature, $\partial \mathbf{a}_{LW,T}/\partial \sigma_{LW}$ as the absorptivity changes with the lw absorption cross-section σ_{LW}, and $\partial \sigma_{LW}/\partial T_E$ as the changes of the cross-section with temperature. So, the first term in (15) describes the growth of $\mathbf{a}_{LW}$ or $\mathbf{a}_T$ with the vapor concentration, which on its own is strongly temperature dependent due to the Clausius-Clapeyron equation; the second term represents the variations of $\mathbf{a}_{LW,T}$ with the absorption cross-section, which changes due to temperature dependent population densities of the involved molecular states and the linewidths (for details see, e.g., Harde-2013 [18]).

The partial derivative $\partial \mathbf{a}_{LW,T}/\partial C_{WV}$ can be found by calculating the absorptivity as a function of the WV concentration and then taking the slope to this curve at a given concentration. Figure 9 displays the lw absorptivity $\mathbf{a}_{WV} = \mathbf{a}_{LW}$ only of water vapor at clear sky via the concentration (lower graph, black diamonds) and on the other hand the total absorptivity $\mathbf{a}_T$ (blue squares) resulting from all GH gases and the clouds. Both graphs were calculated applying an MRT lineshape and in the latter case assuming the global mean cloud cover of 66%, an altitude of 6 km, and an emissivity of 0.48. The pink lines are fits to the absorptivities with logarithmic progression.

In this context it has to be mentioned that the absorptivities, reflecting integrals of the absorption coefficients and, thus, integrals of the cross-sections over the altitude and over the spectral distribution (see Harde-2014 [16], (2–4)), inherently include the general temperature dependence of the absorption coefficients with altitude, but this has to be distinguished from the surface temperature variations, which influence the whole vertical temperature distribution over the atmosphere and which are represented by the second term in (15). The decrease in the WV absorptivity $\mathbf{a}_{WV}$ at an increasing ground temperature from 16 to 21°C at otherwise same conditions is represented by green triangles in Figure 9 for three WV concentrations.

In AR5-WG1-Chap.8.3.1 we can read that most intercomparison studies of the RF of GH gases are for clear sky and aerosol-free conditions, while the introduction of clouds would greatly complicate the targets of research and are usually omitted in the intercomparison exercises of GCM radiation codes and LBL codes. Therefore, obviously also for an assessment of the WV feedback cloud effects were neglected. In addition, most of the GCMs emanate from a mean WV concentration of 7,750 ppm, in agreement with the US Standard Atmosphere 1976, representing mid-latitude but not global mean conditions. The slope to the clear sky WV absorptivity at 7,750 ppm then gives $\partial \mathbf{a}_{WV}/\partial C_{WV} = 0.0018\%/\text{ppm}$, and a WV increase of 7%/°C, as assumed in AR5-WG1-FAQ-8.1, contributes to $\partial C_{WV}/\partial T_E = 542\,\text{ppm}/^\circ C$. Substituting $\mathbf{a}_{LW}$ by $\mathbf{a}_{WV}$ this gives for the first term on the right side of (15) the following:

$$\frac{d\mathbf{a}_{WV}}{dT_E}(1.\,\text{term}) = \frac{\partial \mathbf{a}_{WV}}{\partial C_{WV}} \frac{\partial C_{WV}}{\partial T_E} = 0.98\%/^\circ C \quad (16)$$

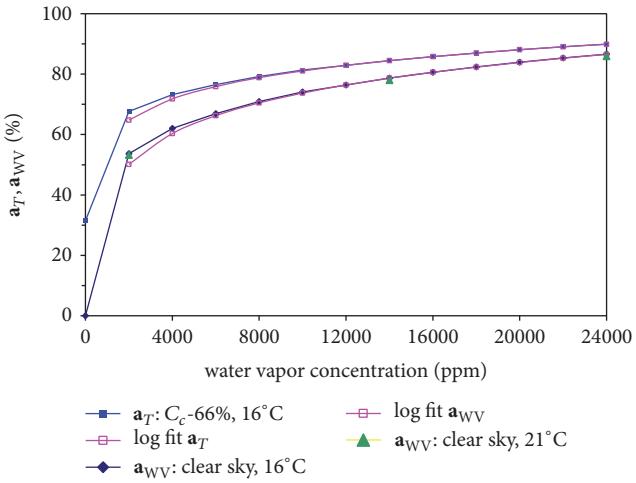

FIGURE 9: Lw water vapor absorptivity $\mathbf{a}_{WV}$ (black diamonds) and total absorptivity $\mathbf{a}_T$ (blue squares) as a function of the WV concentration at a surface temperature of 16°C. The magenta graphs represent logarithmic fits to the absorptivities. Green triangles indicate calculation of $\mathbf{a}_{WV}$ at 21°C.

and is almost exactly the absorptivity change per °C, necessary to deduce a WV feedback of $f_{WV} = 1.6\ W/m^2/°C$ and an amplification factor of two, as published in AR5.

So, under these assumptions the IPCC data can well be reproduced. But as outlined above, this approach omits clouds, emanates from a lower WV concentration, and neglects any surface temperature dependence of the absorption cross-section of the GH gases.

Our own considerations include a spectral overlap and interference of WV with other GH gases as well as with clouds, and we assume a global mean WV concentration (at standard conditions) of 14,615 ppm. Both aspects contribute to a larger total absorptivity $\mathbf{a}_T$, but to a reduced pitch around the mean WV concentration and result in a slope $\partial\mathbf{a}_T/\partial C_{WV} = 0.00042\%/ppm$. Together with a WV increase of 5.9%/°C (see above), which due to the higher WV concentration now contributes to a gain per °C of $\partial C_{WV}/\partial T_E = 862\ ppm/°C$, this gives for the first term in (15) an increase of the total absorptivity of $(d\mathbf{a}_T/dT_E)_{1.\,term} = 0.36\%/°C$.

The temperature variation of $\mathbf{a}_T$ via the absorption cross-section can be found by calculating the absorptivities for different surface temperatures at otherwise identical vapor and gas concentrations. Since for these calculations we assume a fixed temperature at the tropopause of 216.6 K, independent of the surface temperature, any T_E-variations fade with altitude and, thus, also the respective absorptivity changes fade. Therefore, such calculations rather give a lower limit for these changes, yielding a temperature dependence of $(d\mathbf{a}_T/dT_E)_{2.\,term} = -0.08\%/°C$. Inserting this value for the 2nd term in (15), this contributes to a total lw absorptivity change with temperature of

$$\frac{d\mathbf{a}_T}{dT_E} = 0.36 - 0.08 = 0.28\%/°C, \tag{17}$$

which exactly reproduces the result of (13) and was already derived from the slope of Figure 7.

The direct comparison of the different approaches clearly shows the different assumptions and their influence on the WV feedback. Whereas our result only contributes to an increase of the direct CO_2 influence (basic climate sensitivity) of 14%, the IPCC follows from a gain of 100%, which is more than 7 times larger than our result.

4.3.2. Lapse Rate Feedback. The average temperature decrease with altitude over the troposphere is specified as 6.5°C/km and assumed to be constant up to the tropopause at about 11 km altitude [35]. This lapse rate has a direct influence on the power, which is asymmetrically reradiated by the atmosphere in downward and upward direction. In our radiation transfer calculations (see Section 3) this asymmetry is expressed by the parameter f_A, for which at the standard lapse rate we find a back-radiated fraction of about $f_A = 62\%$ and a rejected portion to space of $(1 - f_A) = 38\%$, slightly varying with the individual assumptions like cloud cover, lineshape, or humidity in an RT calculation. When the vertical temperature profile changes and/or the back-radiation varies due to concentration changes of the GH gases with the temperature, as a direct consequence also the radiation balance will be modified. This induces a climatic effect, known as lapse rate feedback.

It is well known that the tropopause height is significantly varying with the climate zone (also over the seasons) and in so far directly related to the local ground temperature. A detailed description of the tropopause altitude and its variation with latitude has been given by Hoinka [56]. While the mean absorption and reradiation over some longer or shorter distance in the troposphere will not noticeably be influenced, as long as the optical depth is the same, changes of the lapse rate with the ground temperature directly affect the back-radiated fraction f_A and, thus, the total balance of EASy. However, due to dominating wet-adiabatic convection in the atmosphere the lapse rate can be expected to a large extent to be the same even at strongly varying surface temperatures. Nevertheless, a remaining variation of f_A with temperature can be observed which is induced by the stronger WV changes with the climate zone and thus with the surface temperature. The green line in Figure 7 displays this variation of f_A with the ground temperature for the case of a constant lapse rate over the three climate zones as well as over the troposphere and supposing a vertical WV distribution in agreement with the Clausius-Clapeyron-equation. Under these conditions we find a temperature dependence of $df_A/dT_E = 0.11\%/°C$ as already specified in (14), which on its own would contribute to a positive lapse rate feedback of $f^+_{LR} = +0.85\ W/m^2/°C$.

On the other side in AR5 we can read "*both theory and climate models indicate that global warming will reduce the rate of temperature decrease with altitude, producing a negative lapse rate feedback that attenuates the greenhouse effect.*"

So, global circulation models predict an enhanced warming in the upper troposphere of tropical regions, particularly in response to an increasing water vapor concentration, which should result in a negative feedback. On the other hand, at mid- to high-latitudes, a larger low level warming is

expected as response to the positive radiative warming, thus, providing a positive feedback, as this is expected from the previous considerations. Since the influence of the tropics is assumed to dominate, in AR4 a resulting negative feedback of $-0.85\,\mathrm{W/m^2/^\circ C}$ was predicted [26, 57], which now has been reduced to $f_{LR} = -0.6\,\mathrm{W/m^2/^\circ C}$ (AR5-WG1-Tab.9.5). In our accounting scheme this corresponds to temperature dependence of the back-radiated fraction of $df_A/dT_E = b_a = -0.078\%/^\circ C$ and is represented in Figure 7 as magenta line.

Since the water vapor has a more or less stronger influence on the lapse rate, both effects are often considered together. For the combined feedback we then find $f_{WV+LR} = -0.18\,\mathrm{W/m^2/^\circ C}$ with an attenuation of 0.95, while the IPCC specifies a value of $f_{WV+LR} = 1.1\,\mathrm{W/m^2/^\circ C}$ with an amplification of the climate sensitivity of 1.47 (AR5-WG1-Chap.9, not differentiated between clear sky or cloudiness).

4.3.3. Surface Albedo Feedback. It is well known that changes to the physical properties of the land surface and sea ice will perturb the climate, both by exerting an RF and by modifying other processes such as the fluxes of latent and sensible heat or the transfer of momentum from the atmosphere. Also the other way round is climate influencing the surface properties, which again act back on the climate. So, an increasing ground temperature reduces the Earth's reflectivity via melting ice shields in the polar regions and it changes the vegetation. With varying reflectivity particularly the sw radiation balance will be modified in such a manner that with reducing sw reflectivity r_{SE} more power is absorbed by the Earth's surface which then contributes to an additional heating of the ground.

This surface albedo influence is estimated as a positive feedback of $f_{SA} = 0.3 \pm 0.1\,\mathrm{W/m^2/^\circ C}$ (AR5-WG1-Tab.9.5). In our simulations we introduce this albedo feedback as a temperature dependent change of the Earth's reflectivity with

$$\frac{dr_{SE}}{dT_E} = -0.143\%/^\circ C, \tag{18}$$

which under clear sky contributes to an increase of the climate sensitivity of 12% and at mean overcast of 10%.

4.3.4. Convection Feedback. Sensible heat represents the energy transfer through thermal conduction and convection from the warmer surface to the colder atmosphere. At the reference CO_2 concentration of 380 ppm and temperature $T_R = 16^\circ C$ this heat flux was chosen to be $17\,\mathrm{W/m^2}$ in agreement with the TFK-scheme, and this flux was assumed to be constant in the previous simulations. However, the driving force for this flux is the temperature difference at the boundary layer between surface and atmosphere. In addition, advection in form of a horizontal energy transfer along the boundary through wind and water currents takes place. This transfer is only indirectly dependent on the temperature difference; therefore, it is close-by to assume a power transfer per surface area, which is represented by a temperature independent portion I_{C0} and a temperature dependent part in the form

$$I_C(T_E, T_A) = I_{C0} + h_c(T_E - T_{AC}), \tag{19}$$

with h_C as the heat transfer coefficient and T_{AC} as the air temperature at the convection zone.

Since in first approximation T_{AC} can be assumed to scale synchronously with the lower atmospheric temperature T_A, typically reflecting a temperature equivalent to an air layer temperature in about 800 m altitude, but convection is only dominant over about 200 m height, the temperature difference $(T_E - T_{AC})$ in (19) is considered to be just one-quarter of the difference $(T_E - T_A)$ (see Harde-2014 [16], Subsections 4.4 and 5.4.4).

Due to the second term in this equation any changes in the surface and atmospheric temperature, which may be induced by CO_2, initiate a feedback on EASy. We call this convection feedback.

From Figure 6(a) we see that under clear sky the air temperature reacts less sensitively to CO_2 variations than the Earth temperature, and the difference $(T_E - T_A)$ increases with rising CO_2 concentration. Therefore, also the sensible heat flux grows with the concentration and contributes to an additional cooling with a negative feedback.

This feedback gets maximum, when the first term on the right side of (19) vanishes and the total heat flux of $17\,\mathrm{W/m^2}$ at 380 ppm CO_2 is determined by the second term. Under regular cloud cover with a temperature difference $(T_E - T_A) = 5.2^\circ C$ the heat convection coefficient can assume a maximum value of $h_{C,max} = 17/0.25/5.2 = 13\,\mathrm{W/m^2/^\circ C}$. When choosing a smaller convection parameter, this automatically reduces the feedback but increases the first term in (19), so that at the reference CO_2 concentration always a sensible heat flux of $17\,\mathrm{W/m^2}$ is guaranteed (for clear sky it gets slightly larger).

From Figures 6(b) and 6(c) we further recognize that with increasing cloud cover the difference in $(T_E - T_A)$ more and more disappears and, thus, any feedback gets smaller.

With $h_{C,max} = 13\,\mathrm{W/m^2/^\circ C}$ we calculate at clear sky a climate sensitivity of $C_S = 1.68^\circ C$ with a feedback of $f_{CO} = -0.19\,\mathrm{W/m^2/^\circ C}$ and an attenuation factor of 0.94, whereas at regular cloud cover the sensitivity turns into $C_S = 1.07^\circ C$ with a feedback of only $f_{CO} = -0.06\,\mathrm{W/m^2/^\circ C}$ and a damping factor of 0.98. With a more moderate convection coefficient of 4–6 $\mathrm{W/m^2/^\circ C}$, as this has to be expected, when some larger fraction of the sensible heat transfer has to be assigned to advective processes, convection feedback still further decreases, and with a damping of less than 1% then this feedback process can well be neglected.

4.3.5. Evaporation Feedback. Latent heat describes the energy transfer resulting from phase transitions of evaporating water or sublimating ice at the surface and their subsequent release of the vaporization energy in the atmosphere, when the water vapor condenses and falls back as precipitation. Similar to sensible heat but even more pronounced this contributes to cooling of the surface. Since an increasing Earth temperature further forces these processes, they also result in a negative feedback, which we call evaporation feedback. Although in

more general terms this is also one part of convection, we further distinguish convection and evaporation feedbacks to assign them to sensible and latent heat contributions.

Generally, according to Kirchhoff's equation (see, e.g., Salby [33], p. 123) changes in latent heat are directly proportional to temperature changes with a proportionality factor, given by the difference of the specific heats in the two phases. To allow some smaller deviations from this general response over a wider temperature interval, and on the other hand to express only changes in latent heat around a point of reference, as this is of particular interest for our considerations, we assume a similar relationship for latent heat as applied for sensible heat with

$$I_L(T_E) = I_{L0} + l_H(T_E - T_0), \tag{20}$$

consisting of a temperature independent contribution I_{L0}, and a second term proportional to the surface temperature above the freezing point $(T_E - T_0)$. l_H is the latent heat transfer coefficient. Under regular conditions I_{L0} almost vanishes, and the feedback, only determined by the second term in (20), gets maximum. Since the total flux at the reference CO_2 concentration of 380 ppm is held fixed to 80 W/m^2 in agreement with the TFK-scheme, at mean cloud cover l_H can assume a maximum value of 5 W/m^2/°C (80 W/m^2 ÷ 16°C), which may also be used under clear sky conditions. When for some reason the heat transfer is less sensitively responding to temperature changes (e.g., less rapidly increasing precipitation rate or saturating evaporation), l_H and by this the feedback can slightly decline. Then, in the same way, as the second term in (20) decreases, the first term increases.

At clear sky and maximum $l_{H,\max} = 5$ W/m^2/°C we find a climate sensitivity of $C_S = 1.06$°C, a feedback of $f_{EV} = -2.1$ W/m^2/°C, and a damping coefficient of 0.59; at mean cloud cover C_S reduces to $C_S = 0.61$°C with a maximum negative feedback of even $f_{EV} = -2.76$ W/m^2/°C and a damping of 0.56. So, latent heat can contribute to significant negative feedback and work as a strong stabilizer for the climate.

Similar results for the convection and evaporation feedback were derived by Andrews et al. [58], who investigated the regression of changes in annual-mean global mean surface heat fluxes against annual-mean global mean ΔT for the first 20 yr after CO_2 was doubled. As an ensemble mean of various GCMs they specify for the sensible heat feedback (here f_{CO}) a slightly positive value of 0.26 W/m^2/°C and for the latent heat feedback (here f_{EV}) a stronger negative value of −2.22 W/m^2/°C. However, it is not clear how these data were deduced, for clear sky or cloudy conditions.

4.3.6. Thermally Induced Cloud Feedback. Clouds respond to climate forcing mechanisms in multiple ways, and differences in cloud feedbacks constitute by far the primary source of spread of both equilibrium and transient climate responses simulated by climate models (Dufresne & Bony [59]). So, in AR5-WG1-Chap.7 we can read as follows: "*the sign of the net radiative feedback due to all cloud types is less certain (than the net feedback from water vapor and lapse rate changes) but likely positive. Uncertainty in the sign and magnitude of the cloud feedback is due primarily to continuing uncertainty in the impact of warming on low clouds. We estimate… the cloud feedback from all cloud types to be +0.6 (−0.2 to +2.0) W m^{-2} °C^{-1}. These ranges are broader than those of climate models to account for additional uncertainty associated with processes that may not have been accounted for in those models.*"

Indeed quite contradictory observations of could effects can be found in the literature, where on the one side regional meteorological conditions over the Pacific are reported, providing modelling evidence for a positive low level cloud feedback in this region on decadal time scales (Clement et al. [60]). On the other side, particularly in the tropics, the opposite trend is observed that with increasing temperature and thus rising humidity also the cloud formation is increasing, which then contributes to negative feedback (Lindzen et al. [61]; Laken & Pallé [62]; Cho et al. [63]; Caldwell et al. [64]).

Different to any detailed investigations, which are focusing on individual contributions of low- or high-level clouds to a feedback, here we concentrate on a more general description, how such a feedback can be derived and quantified from global cloud observations and how it can be incorporated into a climate model. Cloud feedbacks can have different origin and importance, depending on the individual forcings, which are responsible for a rebound on the climate via clouds. In this subsection we look closer to CO_2 as the responsible climate driver, which initiates a temperature increase and might induce a temperature induced cloud feedback (TICF). In Section 5 we additionally investigate the solar influence on clouds and call this solar induced cloud feedback (SICF).

Our preceding simulations, which were performed for clear sky and at cloudiness, already demonstrate the dominant influence of the clouds as part of the total atmospheric convection on the global temperature and the self-adjusting fluxes between the surface, the atmosphere, and space. So, the climate sensitivity drops to about 60% of its value it had at clear sky conditions, and the ground temperature approximately changes from 20 to 16°C, when the cloud cover increases from 0 to 66%. This temperature response was adopted from the ISCCP observations of the global warming and mean cloud cover variations over the period 1983–2010 [22], and this response is also the basis for our further assessment of a temperature induced cloud feedback.

It is obvious that the observed temperature changes will not exclusively result from cloud variations or vice versa but will also be affected by variations of the solar radiation, the humidity, or internal oscillations. Therefore, the worst case will be to attribute any response of the cloud cover C_C, as derived from the ISCCP data, only to the surface temperature change ΔT_E and to address this change only to the CO_2-GH effect (CO_2 induced cloud feedback), this at least around the mean cloud cover of 66% and the mean global temperature of 16°C. Since even at very high temperatures clouds will not completely disappear, we suppose a rest cloudiness of $C_{C,\min} = 20\%$ and an exponential approach to this lower limit. Further, to represent the cloud cover also for negative ΔT_E's, as this is the case for smaller CO_2 concentrations than the reference at 380 ppm, we use for reasons of uniqueness the same functional relation. So, we express the cloud cover as a

function of the ground temperature as (see Harde-2014 [16], (85)):

$$C_C(T_E) = \begin{cases} C_{C,\min} + (C_{CR} - C_{C,\min}) \cdot e^{-c_f (T_E - T_R)/T_R}, & T_E \geq T_R, \\ C_{CR} + (C_{CR} - C_{C,\min}) \cdot \left(1 - e^{c_f (T_E - T_R)/T_R}\right), & T_E < T_R \end{cases} \quad (21)$$

with $C_{CR} = 66\%$ as the mean cloud cover at $T_R = 16^\circ$C and c_f as the temperature induced cloud cover parameter. In principle (21) just describes the reciprocal dependence as used in our two-layer model to derive the ground temperature variation as a function of the cloud cover. It is clear that for too large negative temperature deviations C_C would get larger than 100% and then has to be truncated, but within regular variations this is not the case.

To reproduce the cloud variations in agreement with the ISCCP observations, a cloud cover parameter of $c_f = 5.4$ is required, yielding a cloud cover change of −1% at $\Delta T_E = 0.065^\circ$C. A simulation with this value at mean cloudiness and assuming changes only caused by the CO_2-GH effect gives an equilibrium climate sensitivity of ECS = $C_S = 2.53^\circ$C, corresponding to a feedback $f_{CT} = 2.0\,W/m^2/^\circ C$ and an amplification of 2.3. With this worst case calculation we can just confirm the upper limit for the cloud feedback as estimated by the IPCC (see above). At the same time, however, this result also makes clear that for a reliable assessment of the climate sensitivity particularly reliable data about the driving force and size of any cloud cover changes are important, since they have an exceptionally strong influence on the further conclusions.

In this context it is important to note that a larger assumed temperature response of the model to cloud changes, as this follows from an inverse scatter plot based on the BEST temperatures, has no influence on the feedback parameters and the climate sensitivities, since due to the reciprocity a larger temperature response of the model is compensated by a smaller cloud cover parameter c_f and vice versa. Only when this reciprocity would not exist, as this might be inferred from the direct plot of the cloud fraction versus BEST temperature with cloud changes of only −3%/°C, c_f would reduce to 1.05, which in our model just reproduces the mean cloud feedback of $f_{CT} = +0.6\,W/m^2/^\circ C$ as specified in AR5.

In any case, this distinctly lower feedback therefore indicates that obviously

(i) the observed cloud changes cannot exclusively be traced back to global warming by CO_2, but additional overlaying temperature variations or counteracting processes are present and/or

(ii) the cloud changes are additionally or alone controlled by a further climate forcing mechanism.

We will come back to these aspects in Section 5.

4.3.7. Total Feedback. The main results of our simulations for the individual and collective feedbacks with their effect on the climate sensitivity are listed in Table 10. The upper 10 lines show the data calculated under clear sky conditions and the 14 lower ones the results under mean cloud cover. Comparison of respective rows without and with overcast clearly demonstrates the dominant influence of clouds, causing a significant reduction of the sensitivities, as long as the thermally induced cloud feedback is excluded. So, with water vapor, lapse rate, albedo, and evaporation feedback C_S diminishes to 0.62°C (line 22).

Additionally assuming CO_2 induced cloud feedback with a cloud cover parameter $c_f = 5.4$ and a medium convection feedback ($h_C = 5\,W/m^2/^\circ C$) the climate sensitivity rises to $C_S = 1.22^\circ$C, and the previously observed reduction, compared to clear sky, is almost lost (compare lines 10 and 24). The same mechanism, which reduces the temperature with increasing cloud cover, is also active in opposite direction.

It is also worth noting that with an increasing negative evaporation feedback the convective part, which under mean cloudiness is already quite small (see line 15), is still further pressed down and under special conditions even can get slightly positive. In general, however, when a moderate heat convection coefficient is chosen to allow also advective heat transfer, a convective feedback can completely be neglected. From this behavior we also see that the total feedback is by far not only the sum of the individual contributions.

Due to the above assumptions that the observed cloud changes within the ISCCP program are only thermally induced and the respective temperature increase over this period is only caused by CO_2 (maximum cloud feedback $f_{CT} = 2.0\,W/m^2/^\circ C$), our analysis with all the other feedbacks included shows that a climate sensitivity of $C_S = 1.2^\circ$C obviously represents an upper limit for this quantity. Similar conclusions hold for the response of EASy with a ground temperature variation of 7°C at a 100% cloud cover change. Obviously also paleo-climatic investigations (see, e.g., Petit et al. [2]) indicate that EASy stabilizes itself within temperature variations of about 6-8°C, and this still under the influence of even much stronger solar changes as well as under much larger CO_2 concentrations, as they were found 500 Mio years ago.

With a cloud response of $c_f = 1.05$ ($f_{CT} = +0.6\,W/m^2/^\circ C$, see line 23) the climate sensitivity assumes a moderate value of $C_S = 0.74^\circ$C. Under these conditions the observed warming over the last hundred twenty years of about 0.8°C, which the IPCC almost exclusively assigns to anthropogenic forcing, could only be explained to less than one-half (0.31°C) by the 100 ppm CO_2 increase over this period. That is, most of the observed warming could not follow from anthropogenic forcing. If the warming over the eighties and nineties additionally might have been superimposed by some other thermal processes, for example, an increased solar activity, Pacific Decadal Oscillations (PDO), the Southern Oscillation Index (SOI), or other GH gases, the respective CO_2 initiated contribution to cloud changes further diminishes, which also reduces the feedback and in the same way the climate sensitivity.

As direct comparison to our calculations we have also listed a simulation assuming the feedbacks as used in AR5-WG1-Tab.9.5 with a WV plus lapse rate feedback of

Table 10: Calculated equilibrium climate sensitivities under different feedback conditions.

Line number	Clouds C_C (%)	c_f	Water vapor	Lapse rate b_a (%/°C)	Albedo e_f (%/°C)	Convection h_C(W/m^2/°C)	Evaporation l_H (W/m^2/°C)	Feedback f(W/m^2/°C)	C_S (°C)	Rel.
1	0	—	—	—	—	—	—	0	1.79	1.00
2	0	—	on	—	—	—	—	1.10	2.81	1.57
3	0	—	—	−0.078	—	—	—	−0.47	1.55	0.87
4	0	—	—	—	−0.143	—	—	0.33	2.01	1.12
5	0	—	—	—	—	13	—	−0.19	1.68	0.94
6	0	—	—	—	—	—	5	−2.10	1.06	0.59
7	0	—	on	−0.078				0.62	2.25	1.26
8	0	—	on	−0.078	−0.143	—	—	0.96	2.61	1.46
9	0	—	on	−0.078	−0.143	13	—	0.57	2.20	1.23
10	0	—	on	−0.078	−0.143	5	5	−1.05	1.33	0.74
11	66	0	—	—	—	—	—	0	1.09	1.00
12	66	0	on	—	—	—	—	0.43	1.24	1.14
13	66	0	—	−0.078	—	—	—	−0.60	0.93	0.85
14	66	0	—	—	−0.143	—	—	0.30	1.19	1.10
15	66	0	—	—	—	13	—	−0.06	1.07	0.98
16	66	0	—	—	—	—	5	−2.76	0.61	0.56
17	66	1.05	—	—	—	—	—	0.60	1.31	1.21
18	66	5.4	—	—	—	—	—	1.98	2.53	2.33
19	66	0	on	−0.078	—	—	—	−0.18	1.04	0.95
20	66	0	on	−0.078	−0.143	—	—	0.12	1.13	1.04
21	66	0	on	−0.078	−0.143	13	—	−0.08	1.06	0.98
22	66	0	on	−0.078	−0.143	—	5	−2.64	0.62	0.57
23	66	1.05	on	−0.078	−0.143	5	5	−1.62	0.74	0.68
24	66	5.4	on	−0.078	−0.143	5	5	0.37	1.22	1.12
AR5	66	1.05	f_{WV+LR} = 1.1 W/m^2/K		−0.143	—	—	2.18	2.93	2.70

f_{WV+LR} = 1.1 W/m^2/°C, ($d\mathbf{a}_{WV}/dT_E$ = 0.98%/°C, $df_A/dT_E = b_a$ = −0.08%/°C), an albedo feedback of f_{SA} = 0.3 W/m^2/°C (e_f = −0.143%/°C), and a cloud feedback (see AR5-WG1-Chap.7) of f_{CT} = 0.6 W/m^2/°C (c_f = 1.05). With these parameters we find a climate sensitivity of C_S = 2.9°C, which is 10% smaller than the model mean of the CMIP5 AOGCMs and essentially results from our smaller Planck sensitivity (see Table 8), but otherwise reproduces the AOGCMs very well. So, the big discrepancy between the IPCC's accounting scheme and ours can clearly be identified to originate from the negative WV lapse rate feedback and the negative evaporation feedback considered in our calculations.

Altogether, we see that the dominating positive feedbacks, originating from clouds and albedo, are partially compensated or in the case of a moderate cloud feedback are even overcompensated by negative WV lapse rate and evaporation feedback. Particularly clouds have two stronger opposing influences on the energy balance, which can neutralize each other or can even have an overall attenuating impact on the ECS, dependent on the mechanisms responsible for cloud changes.

So, up to now it is not clear if the ISCCP observations are really only a consequence of the increased temperature as assumed in Section 4.3.6 or at least to some degree are stimulated by nonthermal solar activity over the observation period (Ziskin & Shaviv [11]; Vahrenholt & Lüning [25]; Svensmark et al. [23, 65, 66]; Enghoff et al. [67]; Kirkby et al. [68]). In the latter case the strong thermal cloud feedback had to be cancelled with the effect that at otherwise same conditions the climate sensitivity would drop to about 0.6°C.

An important criterion for a serious validation, which mechanism really might control the cloud cover changes, we can derive from model simulations, which additionally include the solar anomaly over the last century and compare this directly with the observed global warming over this period. Similar investigations have been performed by Ziskin and Shaviv [11], where they show that obviously such solar induced component is necessary to reproduce the 20th century global warming and that the total solar contribution is much larger than can be expected from variations of the total solar irradiance (TSI) alone.

To verify the existence and size of such a solar effect in the total energy budget we have performed quite similar analyses,

which also include solar variations and orientate at the observed warming over the last century, but which are based on our two-layer model, including all discussed feedback processes and especially reproducing the ISCCP observations of cloud cover changes. Of course, any conclusions deduced from such comparison sensitively depend on the reliability of the measured cloud cover, the solar activity, and temperature changes over this period.

5. Solar Influence

In the same way as the GH gases have an influence on the radiation and energy budget of EASy, this is the case for a varying solar activity. Both are external perturbations, causing an imbalance, to which EASy has to respond with a new distribution for the respective temperatures at the surface and in the atmosphere.

Such response on a varying solar activity can easily be simulated with our two-layer climate model by changing the solar constant (total solar irradiance, TSI) or the average solar flux in our parameter list in Table 6. So, a simulation with a 0.1% larger TSI contributes to an increase of the surface temperature of 0.09°C. In analogy to the CO_2 climate sensitivity we may call this the solar sensitivity S_S. Typically, over a Schwabe cycle (11 years) variations of the solar constant of 0.1–0.12% are observed, corresponding to an equilibrium temperature change of about 0.1°C.

But for a serious assessment of the solar influence on global warming we further have to discuss two contributions, which can modify the basic solar sensitivity S_S:

(i) an amplification by a possible temperature induced cloud feedback, which works in the same way as discussed for the CO_2 induced cloud feedback but now results from the solar heating, and

(ii) a temperature independent mechanism, which acts back on the cloud formation when the solar activity is changing and in this way contributes to an amplification of S_S. We call this a solar induced nonthermal cloud feedback.

We first look to their individual contributions before we unify them in a common model which orientates at the global warming over the last century and allows an assessment of the influence of the two climate drivers, the CO_2, and the Sun, on our climate.

5.1. Thermally Induced Cloud Feedback. When a thermally induced cloud feedback (TICF), as discussed in Section 4.3.6, is assumed to be responsible for the observed cloud cover changes, this feedback also has to be applied to the direct solar initiated warming. Here we focus only on CO_2 and solar induced contributions, while other effects caused by internal oscillations or volcanic activities are neglected. For the climate and solar sensitivity this should rather give an upper limit. Their individual contributions and, therefore, their relative weighting can be derived, comparing the CO_2 fraction with the respective solar part, including all feedback processes.

With a thermal cloud response of $c_f = 5.4$ and for 100 ppm CO_2 increase we calculate a maximum temperature growth of 0.52°C corresponding to a climate sensitivity of C_S = 1.22°C. The solar part can be assessed from an analysis of Shapiro et al. [10] of long-term solar activity proxies over the last century, which shows an increase of the TSI of slightly more than $\Delta E_S = 0.3\%$ in good agreement with the observed decadal group sunspot numbers over this period (see Hoyt & Schatten [8], updated by Scafetta & Willson [12]). These results are remarkably well confirmed by a new adjustment-free physical reconstruction of solar activities (Usoskin et al. [13]), which indicates a modern Grand maximum (during solar cycles 19–23, that is, 1950–2009) and is found to be a rare or even unique event, in both magnitude and duration, in the past three millennia. Also an actual composite by Soon et al. [15] of the Northern Hemisphere temperature trend, which is mainly based on rural data, supports a stronger influence and variation of the TSI over the last century. So, assuming a solar anomaly of $\Delta E_S = 0.3\%$ this donates a temperature increase of 0.31°C, which in this case corresponds to a solar sensitivity of $S_S = 0.1$°C. The relative contributions of CO_2 and the Sun then behave as about 60 to 40%.

Both together give a warming over the last century of 0.83°C which is slightly more than the observed temperature boost over the last 120 years of 0.74°C (GISS [69]). Although meanwhile the IPCC emanates from a larger global warming of 0.85°C, we refer to the original value of [69], which is in good agreement with the single longest dataset available, yielding a total increase between the average of the 1850–1900 period and the 2003–2012 period with 0.78°C (AR5-WG1-SPM). From Soon et al. [15] we even deduce an increase over the last century of only slightly less than 0.7°C.

Only with a reduced solar anomaly of $\Delta E_S = 0.22\%$, yielding a solar contribution of 0.22°C, or also with a further increased negative feedback the temperature balance could again be satisfied. Without the negative evaporation and convection feedbacks the warming would be completely unrealistic with 1.6°C for CO_2 plus 1.2°C for solar heating. So, well knowing that the observed warming does not represent an equilibrium state, different to our calculations, and can further be superimposed by other effects like the PDO and SOI (see, e.g., Spencer & Braswell [70]), it looks like that a thermal cloud feedback of $f_{CT} = 2\ W/m^2/°C$ ($c_f = 5.4$) appears too high.

On the other hand using a cloud feedback as assumed by the IPCC with $f_{CT} = 0.6\ W/m^2/°C$ ($c_f = 1.05$) the CO_2 contribution declines to 0.31°C and the solar part to 0.17°C. Then their sum is too small to explain the observed warming. However, in any case is such reduced thermal cloud feedback no longer in agreement with the observed cloud changes. As a consequence we state the following: either a maximum thermal cloud feedback of $f_{CT} = 2.0\ W/m^2/°C$ ($c_f = 5.4$) has to be assumed, this at a reduced solar anomaly and/or a further increased negative feedback, or at least some fraction of the cloud cover is also influenced by nonthermal cloud cover changes.

5.2. Solar Induced Cloud Feedback. Since the amount of clouds varies over the solar cycle, there exists strong evidence that the solar activity variations also modulate the cloud cover. Actual publications of Svensmark [23, 65–67] indicate that with an increasing solar activity and, therefore, an increasing solar magnetic field the cosmic flux, which hits the atmosphere, is reduced and causes a direct feedback on the cloud cover. So, it is expected that the generation rate of aerosols as condensation seeds for the formation of water droplets in the lower atmosphere is directly influenced by the cosmic radiation flux (see also cloud experiment, Kirkby et al. [68]), which therewith also controls the cloud cover.

Another proposed mechanism is hypersensitivity of the climate system to ultraviolet (UV) radiation, which typically varies 10x stronger over a solar cycle than the TSI (Haigh [24, 71]; Soon et al. [72]; Haigh et al. [73]). So, increased UV radiation activates the stratospheric ozone production and heat transfer, which via atmospheric waves can further induce sea surface temperature and/or tropospheric circulation variations and in this way also modulate the cloud cover (Kristjánsson et al. [74]).

Obviously both these mechanisms play a role, depending on the climatic conditions and altitude (Voiculescu et al. [75]). Due to their close interrelation here we consider them as a unique effect.

A reduced cloud formation at an increased solar activity then reinforces the initial TSI induced temperature increase and can be included in the 2LCM as a feedback term similar to the thermally induced cloud changes, but now depending on changes of the solar constant, supposing that variations in E_S initiate reciprocal changes in the cloud cover with (see Harde-2014 [16], 86):

$$C_C(E_S) = \begin{cases} C_{C,\min} + (C_{CR} - C_{C,\min}) \cdot e^{-s_f (E_S - E_{SR})/E_{SR}}, & E_S \geq E_{SR}, \\ C_{CR} + (C_{CR} - C_{C,\min}) \cdot \left(1 - e^{s_f (E_S - E_{SR})/E_{SR}}\right), & E_S < E_{SR}. \end{cases} \quad (22)$$

where E_{SR} is the mean solar constant as a reference and s_f the solar induced cloud cover parameter.

Assuming that the cloud cover variation over the period 1983–2000 of −4% is only determined by an observed increase of the TSI of δE_S = 0.1% (Willson & Mordvinov [9]), this results in a feedback parameter s_f = 90. It should be noticed that a smaller supposed increase of the TSI over this period (designated as δE_S) and therefore deviating from Willson & Mordvinov only pushes the parameter s_f further up and increases the solar feedback.

With this additional solar induced cloud feedback (SICF) the basic solar sensitivity of 0.09°C rises to S_S = 0.31°C. However, in the same way as any warming causes further feedback processes, as discussed in Section 4.3.7, also warming according to solar stimulated cloud changes will further be amplified or attenuated. With all feedbacks included in this case we find a solar sensitivity of S_S = 0.18°C, which then replaces the previously specified value, derived under conditions of TICF.

When SICF is the only responsible process controlling the cloud cover, also for the CO_2 climate sensitivity TICF has to be cancelled and C_S reduces to 0.66°C.

With a solar anomaly of ΔE_S = 0.3% and a solar sensitivity of S_S = 0.18°C this already gives a temperature increase of 0.51°C (slightly nonlinear), which is 0.2°C more than the solar contribution for pure TICF (see Section 5.1). On the other hand CO_2 with an increase of 100 ppm over this period (and applying the respective climate sensitivity of C_S = 0.66°C, now without TICF) then only delivers additional 0.28°C. The sum with 0.79°C again gives a slightly too high growth over the last 120 years. However, with a smaller solar anomaly, in this case of 0.27% over this period, the warming can exactly be reproduced. Under these conditions the Sun contributes 69% to global warming and CO_2 the rest.

Similar to Shapiro et al. [10], Hoyt & Schatten [8], Scafetta & Willson [12], Usoskin et. al. [13], and Soon et al. [15] a larger solar influence on global warming has also been reported by Zhao and Feng [14], who have investigated the periodicities of the solar activity and the Earth's temperature variation on a time scale of centuries, using the wavelet and cross correlation analysis techniques. From this they conclude that during the past 100 years solar activities display a clear increasing tendency which correlates very well with the global warming of the Earth, including land and ocean.

If the solar anomaly (related to the last century) should have been overestimated and would only be ΔE_S = 0.1% (see Wenzler et al. [76]), it has to be expected that also δE_S is declining, for example, to 0.05%. Then, with s_f = 180, the solar fraction still contributes more than 50% to global warming.

Here we do not discuss any additional influence of aerosols over this period, since any reliable figure of such effect is largely unknown and is not the subject of feedback processes. Implicitly aerosols are already enclosed in our model via atmospheric and cloud backscattering, so that any aerosol impact could easily be modelled by varying the sw backscattering parameters and if necessary also the cloud absorption.

5.3. Combined Solar and Thermally Induced Cloud Feedback. The previous investigations have made clear that the measured cloud cover changes by the ISCCP cannot satisfactorily be explained by a pure thermal mechanism. Either this gives too high global warming over the last century, or with the IPCC's favored cloud feedback it results in a too small cloud cover variation over the eighties and nineties. Also a pure solar induced nonthermal cloud feedback with a solar anomaly of ΔE_S = 0.3% results in a slightly too high global warming. So, in both cases, some smaller corrections in the solar variability and/or the total feedback would be necessary to satisfy all constraints.

On the basis of our investigations reasons for a still stronger negative feedback are not so much expected, although we always assumed a more conservative assessment, for example, excluding an internal variability with its influence on the global temperature and cloud effects. This would even further increase the discrepancy to the IPCC's assessment of the ECS. However, larger uncertainties exist for the solar anomaly over the last century and its influence on

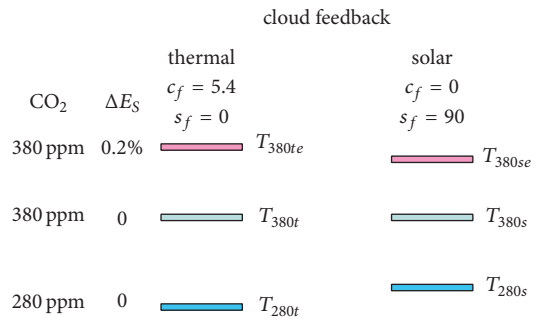

Figure 10: Designation of the temperatures required for calculating global warming due to CO_2 and solar variations by means of a mixed model considering thermal and solar cloud feedback.

cloud cover changes. Since the size of this anomaly has far reaching consequences on both cloud changing mechanisms, it is necessary to consider this influence in more detail, and as long as it is not clear which of these mechanisms is the dominating feedback process it is even reasonable to discuss a combination of these effects.

One way to handle the simultaneous presence of TICF and SICF is to modify the thermal and the solar induced cloud cover parameters c_f and s_f which then determine the weighting of a mechanism relative to their maximum values. The other possibility is to leave the cloud parameters fixed at their predetermined values for a cloud cover change in agreement with the observations and then directly weighting the two feedback processes, which together have to satisfy the constraints for global warming and cloud cover changes. Both procedures give similar results, but the second appears more straightforward and was preferred in our further simulations. The principal accounting scheme can be retraced from Figure 10.

First the weighting factor for the thermal to solar feedback has to be calculated, which specifies an additional admixture of the thermally induced cloud cover changes to the solar initiated changes, this with the objective to satisfy the warming balance over the last century. This weighting should not be mixed with the fraction of the CO_2 initiated to the solar created warming, which can finally be derived as one important result of this calculation model. The weighting requires determining the temperature at 380 ppm CO_2 with increased TSI (T_{380se}), then at 280 ppm and regular TSI (T_{280s}), both for $c_f = 0$ and $s_f = 90$ (only solar induced) and including all other feedbacks. Their difference $T_{380se} - T_{280s}$ gives the total warming caused by CO_2 and the Sun under conditions with only the nonthermal SICF present (see Section 5.2). The same procedure is repeated for $c_f = 5.4$ and $s_f = 0$, yielding the total warming $T_{380te} - T_{280t}$ caused by CO_2 and the Sun with only TICF active (Section 5.1). The difference between the observed warming over the last century $\Delta T_{\text{cent}} = 0.74^{\circ}\text{C}$ and the nonthermal contribution, this in relation to the difference between thermal and nonthermal contributions, determines the weighting W_{th} of the thermally induced cloud cover changes. The respective compliment to one gives the solar induced part W_{sol} as follows:

$$W_{\text{th}} = \frac{\Delta T_{\text{cent}} - (T_{380se} - T_{280s})}{(T_{380te} - T_{280t}) - (T_{380se} - T_{280s})}; \qquad W_{\text{sol}} = 1 - W_{\text{th}}. \tag{23}$$

Further multiplying the temperature difference between 380 and 280 ppm CO_2 at regular TSI ($c_f = 5.4$ and $s_f = 0$) with the thermally induced weighting, then multiplying the respective difference at $c_f = 0$ and $s_f = 90$ with the nonthermally induced weighting, and taking the sum of these two products finally gives the CO_2 portion to global warming as follows:

$$\Delta T_{\text{cent}}^{CO_2} = (T_{380t} - T_{280t}) \cdot W_{\text{th}} + (T_{380s} - T_{280s}) \cdot W_{\text{sol}}. \tag{24}$$

The equivalent procedure now at fixed CO_2 concentration but with the differences between increased and regular TSI gives the solar contribution to global warming as follows:

$$\Delta T_{\text{cent}}^{\text{Sun}} = (T_{380te} - T_{380t}) \cdot W_{\text{th}} + (T_{380se} - T_{380s}) \cdot W_{\text{sol}}. \tag{25}$$

Within regular bounds the sum of the CO_2 and solar induced warming then should reproduce the measured warming over the last century, while satisfying the observed ISCCP cloud cover changes.

The respective climate sensitivity is found from the maximum ECS (full TICF) times the thermal weighting, plus the minimum ECS (no TICF) times the solar weighting as follows:

$$C_S = C_S^{\text{TICF}} \cdot W_{\text{th}} + C_S^{\text{no TICF}} \cdot W_{\text{sol}}. \tag{26}$$

The solar sensitivity can be derived from the temperature growth at increasing TSI and with TICF times the thermal weighting, plus the temperature rise due to SICF times the solar weighting and all this normalized to the increased solar activity ΔE_S as follows:

$$S_S = [(T_{380te} - T_{380t}) \cdot W_{\text{th}} + (T_{380se} - T_{380s}) \cdot W_{\text{sol}}] \cdot \frac{0.1\%}{\Delta E_S}. \tag{27}$$

Some typical results based on this combined accounting scheme are compiled in Table 11. All simulations include the previously discussed feedback effects with parameters for the WV, lapse rate, albedo, convection, and evaporation feedback as specified in Table 10, line 24.

Table 11: Calculations for the climate and solar sensitivity with the extended accounting scheme (combined thermally and solar induced cloud feedback) for different solar anomalies ΔE_S and including all feedbacks (see Table 10, line 24).

Line #	ΔE_S %	Weighting (%) Therm.	Solar	c_f	s_f	$\Delta T_{cent}^{CO_2}$ (°C)	ΔT_{cent}^{Sun} (°C)	C_S (°C)	S_S (°C)
1	0.20	100	0	5.4	90	0.52	0.20	1.22	0.10
2	0.21	100	0	5.4	90	0.52	0.21	1.22	0.10
3	0.22	100	0	5.4	90	0.51	0.23	1.22	0.10
4	0.23	82.4	17.6	5.4	90	0.47	0.27	1.12	0.12
5	0.24	64.8	35.2	5.4	90	0.43	0.31	1.02	0.13
6	0.25	43.4	56.6	5.4	90	0.38	0.36	0.90	0.14
7	0.26	13.8	86.2	5.4	90	0.31	0.43	0.74	0.16
8	**0.263**	**7.6**	**92.4**	**5.4**	**90**	**0.30**	**0.44**	**0.70**	**0.17**
9	0.27	0	100	5.4	90	0.28	0.46	0.66	0.17
10	0.28	0	100	5.4	90	0.28	0.48	0.66	0.17
11	0.29	0	100	5.4	90	0.28	0.50	0.66	0.17
12	0.30	0	100	0	90	0.28	0.51	0.66	0.17
13	0.30	100	0	5.4	0	0.52	0.31	1.22	0.10

Whereas the last two rows in Table 11 reproduce calculations as already discussed in Sections 5.1 and 5.2 with an anomaly $\Delta E_S = 0.3\%$ and assuming pure TICF or SICF (both do not satisfy the temperature balance), the extended model shows full agreement with all constraints, as long as the solar anomaly is within the bounds $0.22\% \leq \Delta E_S \leq 0.27\%$. This interval reflects the slightly different temperature response on thermally or solar induced cloud feedbacks while considering the same cloud cover variation. Therefore, the temperature as well as the cloud cover balance can exactly be satisfied within these bounds with the right weighting for the thermal to solar cloud effect.

With an anomaly of $\Delta E_S = 0.22\%$ the global warming over the last century can exclusively be explained by thermal cloud cover changes. Then CO_2 contributes 0.51°C to the warming and the Sun 0.23°C. In this case the climate sensitivity gets maximum with $C_S = 1.22$°C and the solar sensitivity minimum with $S_S = 0.1$°C. On the other hand for $\Delta E_S = 0.27\%$ we just find the opposite situation with $C_S = 0.66$°C, $S_S = 0.17$°C and a CO_2 to solar ratio of 38/62.

In this context it should be noticed that a larger assumed warming over the last century, for example, 0.85°C as considered by the IPCC, leaves the minimum or maximum possible ECS values unchanged; only the bounds for an appropriate solar anomaly satisfying the constraints are shifted to larger values.

The above calculations indicate (different to our previous studies, Harde-2014 [16]) that as long as the solar variability is not better known, we cannot clearly infer which of the cloud changing mechanisms is dominating, and thus which is the right ECS, although SICF fits much better than TICF for an expected solar anomaly of 0.3%.

A reasonable reference for thermally induced cloud changes, however, may be derived from AR5-WG1-Chap.7, where the cloud feedback is estimated as $f_{CT} = 0.6\ W/m^2/°C$, equivalent to a cloud cover parameter $c_f = 1.05$ (see also Section 4.3.6). With all the feedbacks as listed in Table 10, line 23, we found an ECS of 0.74°C. But this cloud feedback was not large enough to explain the ISCCP observations (see Section 5.2, last paragraph). When applying the extended accounting scheme now we can well reproduce the respective climate sensitivity for a solar anomaly of $\Delta E_S = 0.26\%$ (see Table 11, line 7). Under these conditions TICF supplies 13.8% and SICF 86.2% to the cloud cover changes. Then CO_2 contributes 0.31°C and the Sun 0.43°C to the warming over the 20th century.

From these studies we conclude that the measured temperature increase of 0.74°C over the time 1880–2000 and the observed cloud changes of −4% over the period 1983–2000 can best be explained by a cloud feedback mechanism, which is dominated by the solar influence, whereas thermally induced contributions only should have a minor influence.

While a cloud feedback, as estimated in AR5 together with the other feedbacks found in this paper, results in an ECS = 0.74°C, a solar anomaly of 0.27% or larger, as expected from Hoyt & Schatten [8] or Shapiro et al. [10], suggests an even smaller ECS = 0.66°C. Therefore, it seems quite reasonable to use a model mean of $C_S = 0.7$°C, yielding a CO_2 initiated warming of 0.3°C and a solar contribution of 0.44°C (see Table 11, line 8).

A plot of the temperatures T_E and T_A as a function of the CO_2 concentration for $C_S = 0.7$°C is shown in Figure 11. Again the surface temperature can well be represented by a logarithmic graph.

5.4. Discussion and Assessment of Results. Our two-layer climate model together with the integrated radiation transfer calculations show good agreement with the AOGCMs so far, as the Planck sensitivity and the basic ECS only deviate by less than 10%, where these deviations can well be explained

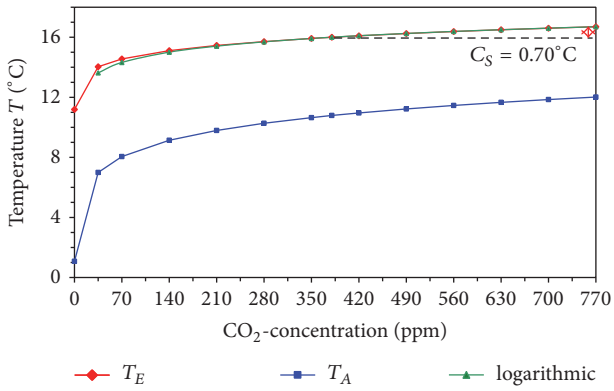

FIGURE 11: Earth temperature T_E (red) and lower tropospheric temperature T_A (blue) as a function of the CO_2 concentration for a solar anomaly of 0.263% yielding C_S = 0.7°C. The green line is a logarithmic approximation.

by the different concepts for calculating the key parameters (in our case the sw and lw absorptivities as well as the back-radiated fraction of the atmosphere, for the AOGCMs the CO_2 radiative forcing) or by different radiation and energy budget schemes, to which the models are calibrated. Also a simulation with the same feedback parameters as compiled in AR5 reproduces the model mean ECS of the CMIP5 AOGCMs within these bounds (see AR5-WG1-Tab.9.5). So, despite very distinctive accounting schemes, this with respect to the concepts, and the expenditure, obviously our simulations give quite reliable results, at least as long as the GCMs can be assumed to be reliable references.

The big discrepancies, however, originate from the differently quantified WV feedback, and on the other side from the neglect of additional feedback processes, which are of fundamental importance for the stabilization of the climate system and which are obviously ignored or not explicitly discussed in AR5.

As outlined in Section 4.3.1 the differences in the WV feedback go back to four main aspects:

(i) We also consider sw WV absorptivity in the atmosphere, which reduces solar absorption at the ground and generates a negative feedback contribution, which cannot be identified in AR5.

(ii) Our LBL-RT calculations for the lw WV absorptivity are valid for mean cloudiness, consider saturation and interference effects with other GH gases, and they use MRT lineshape profiles.

(iii) We emanate from a WV concentration (based on satellite data), which is almost a factor of two larger than that applied in many other calculations. The higher concentration causes a stronger saturation of the WV absorptivity and thus results in a reduced sensitivity to temperature induced concentration changes.

(iv) We additionally include a declining lw WV absorptivity at increasing atmospheric temperatures.

Altogether this results in an amplification due to WV feedback of only 14%, whereas the IPCC assumes a gain of 100%, which is more than 7 times larger. The combined WV lapse rate feedback is even slightly negative with f_{WV+LR} = −0.18 W/m^2/°C (attenuation factor of 0.95).

While the spectral data of the HITRAN-database [20] used for the RT calculations are classified with very high confidence, larger deviations are found for the humidity, which we estimate to contribute to an uncertainty in the feedback of about 10%. But irrespective of the differences in humidity it is not clear why the other contributions are obviously omitted in the IPCC considerations.

The same holds for the convection and evaporation feedback, which together produce significant negative feedback. So, it is without any doubt that, in an energy balance scheme including sensible and latent heat, these fluxes will directly be influenced by surface temperature variations. Respective changes then have to be integrated as feedback processes in an ECS calculation, and, slightly dependent on the assumed advective flux as well as the used radiation and energy budget scheme (see, e.g., Trenberth et al. [21] or Wild et al. [77]); this causes an additional spread in the feedbacks which we also estimate with about 10%.

Considerably larger uncertainties result from cloud feedbacks with different cloud mechanisms, which constitute by far the primary source of spread in the ECS calculations. When any solar anomaly is completely neglected, this in contradiction to several references (see, e.g., Hoyt & Schatten [8], Willson & Mordvinov [9], Shapiro et al. [10], Ziskin & Shaviv [11], Scafetta & Willson [12], Usoskin et al. [13], Zhao & Feng [14], or Soon et al. [15]), the worst case with respect to global warming by CO_2 is to attribute the observed ISCCP cloud changes only to CO_2 with a maximum thermally induced cloud feedback of f_{CT} = 2 W/m^2/°C (upper bound in AR5) and to exclude all other influences like PDO, SOI, or other GH gases. For this rather improbable scenario we calculate a maximum climate sensitivity of C_S = 1.22°C (see Table 10, line 24), which is still well below IPCC's specified range (AR5-WG1-SPM, p. 16) because of the smaller WV feedback and the inclusion of convection and evaporation feedback. But this pure TICF together with the other effects can only explain 0.52°C of the warming over the last century.

Assuming the IPCC's most likely value for the cloud feedback with f_{CT} = 0.6 W/m^2/°C (c_f = 1.05), the climate sensitivity even reduces to C_S = 0.74°C. With this feedback then neither the warming nor the observed cloud cover changes can be explained by a pure thermal effect but require an additional mechanism and/or forcing. Thus, additionally including a solar induced cloud variation over the last century in combination with this thermally induced cloud feedback, all constraints for the temperature variation over the period 1880–2000 and the cloud cover changes from 1983 to 2000 can be satisfied for a solar anomaly of 0.26%.

Since from Hoyt & Schatten [8] or Shapiro et al. [10] an even larger solar anomaly can be expected, which further reduces the ECS, we finally derive a model mean ECS of C_S = 0.7°C and a solar sensitivity S_S = 0.17°C, all in full agreement with the constraints. Then CO_2 contributes 0.3°C (40%) and

the Sun 0.44°C (60%) to global warming over the last century (see Table 11, line 8).

Due to the larger spreads in the solar anomaly and the cloud cover changes we find a maximum range for the ECS of 0.6°C to 1.2°C but with a most reasonable value of $C_S = 0.7$°C.

The deviation to our previous publication ($C_S = 0.6$°C) is explained to mostly result from our new radiation transfer calculations, which much better consider the influence of clouds, and they are determined by the small variations of the atmospheric back-radiation with CO_2 concentration changes.

Our calculations in principle confirm the investigations of Ziskin and Shaviv [11], who attribute 40% of global warming to the solar influence and 60% to other activities. The higher solar and therefore smaller CO_2 portion in our case is explained by the different feedback contributions and also additional feedback processes, which for the ECS are deduced from our own calculations and for the solar sensitivity refer to the cloud changes in the eighties and nineties. In addition, our calculations only represent an equilibrium state of EASy, whereas Ziskin et al. derive their data from a multidimensional fit to the temperature evolution over the last century.

We assert that our result is also in good agreement with Lindzen and Choi [28], who estimated the climate sensitivity from observations, using the deseasonalized fluctuations in sea surface temperatures and the concurrent fluctuations in the TOA outgoing radiation from the ERBE and CERES satellite instruments. With a quite different approach based on the mainly rural temperature trend of the Northern Hemisphere and considering an TSI increase as described by Scafetta & Willson [12], Soon and Connelli even deduce from their calculated residual temperature trends a climate sensitivity of only 0.44°C [15]. From an irreducibly simple model and only critically referring to published data from AR4 and AR5, Monckton et al. [78] also conclude that an ECS smaller than 1°C seems quite likely.

Finally it should be emphasized that in their scenarios the IPCC emanates from the assumption that the actually observed CO_2 increase is almost exclusively determined by the 4% of anthropogenic emissions, while the 96% of natural production over a year is considered to be absolutely independent of any solar or temperature variations, this in contradiction to paleoclimatic investigations (e.g., Petit et al. [2]; Monnin et al. [3]; Caillon et al. [4]; Torn and Harte [5]), which show a delay in the CO_2 emission rate to the temperature of about 800 years, and this also in discrepancy to actual observations of Humlum et al. [6] and Salby [7] with a delay of about 9 months. Assuming the more plausible case that the CO_2 increase of 100 ppm over the last century was caused on the one hand by the 4% anthropogenic emissions and on the other hand by a temperature dependent native emission and absorption rate, then the 4% just contribute 15 ppm to the total CO_2 concentration of 380 ppm and 15% to the 100 ppm increase (for details see Harde-2016 [79]). So, with a CO_2 induced global warming of about 0.3°C over the last century not more than 0.05°C should be caused by human activities.

6. Conclusion

The equilibrium climate sensitivity ECS as the key parameter for an evaluation of the influence of CO_2 on our climate is still one of the most controversially discussed quantities in climate sciences. Calculations of this measure diverge by more than a factor of 10 starting at about 0.4°C and ending at more than 8°C. Also the actual IPCC assessment report, which mainly refers to AOGCM calculations within the CMIP5 program, still specifies this quantity with a relatively wide range of 1.5°C to 4.5°C. Due to the far reaching consequences for future climate predictions it is extremely important to better understand and to discover some of the large discrepancies between different accounting methods applied for this measure. Therefore, in this contribution, we have tried to scrutinize some of these discrepancies by comparing the main steps of the IPCC's preferred accounting system with our advanced two-layer climate model (2LCM), which is especially appropriate to calculate the influence of increasing CO_2 concentrations on global warming as well as the impact of solar variations on the climate (Harde-2014 [16]). It describes the atmosphere and the ground as two layers acting simultaneously as absorbers and Planck radiators, and it includes additional heat transfer between these layers due to convection and evaporation. It also considers short wave (sw) and long wave (lw) scattering processes at the atmosphere and at clouds as well as all common feedback processes like water vapor, lapse rate, and albedo feedback but additionally takes into account temperature dependent sensible and latent heat fluxes as well as a temperature induced and solar induced cloud cover feedback.

As an expansion of our previous investigations we present here detailed line-by-line radiation transfer calculations for the GH gases water vapor, carbon dioxide, methane, and ozone, this under clear sky, at regular cloudiness, at different ground temperatures and humidity, and for different line-shapes. From these calculations we derive the CO_2 radiative forcing as the main parameter in most climate models, also in the IPCC accounting scheme, and additionally we get from these calculations the sw and lw absorptivities as well as the back-radiated fraction of the atmospheric emission, which are the key parameters in our model.

We find quite good agreement for the Planck sensitivity and the basic climate sensitivity, which match within 8% with the model mean of the AOGCMs; however big discrepancies show up for the ECS, when feedbacks are included. While the lapse rate and albedo influence are adopted from literature, the water vapor feedback is derived from the sw and lw absorptivity calculations performed for three climate zones with different surface temperatures and humidity. With a feedback of 0.43 W/m^2/°C and an amplification at mean cloud cover of 1.14 these values are significantly smaller than compiled in AR5 with $f_{WV} = 1.6 \pm 0.3$ W/m^2/°C and an amplification factor of two.

Since our calculations show that with increasing CO_2 concentration the air temperature is less rapidly increasing than the surface temperature, the sensible heat flux at the bound of both layers rises with the concentration. As a consequence more thermal energy is transferred from the

surface to the atmosphere. Similarly, with increasing surface temperature also evaporation and precipitation are increasing with the ground temperature. Both these effects contribute to negative feedback and are additionally included in the simulations. While the respective contribution due to sensible heat rapidly declines with increasing cloudiness, the evaporation feedback absolutely dominates with $f_{EV} = -2.76\ W/m^2/^\circ C$ and is the most stabilizing effect for the temperature restriction with a damping of 0.56.

A special situation is found for the influence of clouds on the radiation and energy budget. Different to any detailed investigations, which are focusing on individual contributions of low- or high-level clouds to a feedback, here we concentrate on a more general description, how such feedback can be derived and quantified from global cloud observations and how it can be incorporated into a climate model. From these observations over a period of 27 years it is deduced that the global mean temperature is increasing with decreasing cloud cover (ISCCP [22]). However, it is not clear if a lower cloud cover is the consequence of the increasing temperature or if the cloud cover is influenced and at least to some degree controlled by some other mechanism, particularly solar activities. In the first case a strong amplifying temperature induced cloud feedback had to be considered, this for the climate sensitivity as well as for a respective solar sensitivity, whereas in the other case the temperature induced cloud effect would disappear for both sensitivities and only a solar induced cloud feedback had to be included due to the solar influence.

A deliberate approach which mechanism really controls the cloud cover is derived from model simulations, which additionally include the solar effect and compare this with the measured temperature increase over the last century. These simulations, considering both effects, show that the observed global warming of 0.74°C (GISS [69]) can best be explained, when a temperature feedback on clouds only has a minor influence. Otherwise the calculated warming would be larger than observed, or the thermally induced cloud feedback would have been overestimated. With a solar anomaly of 0.26% and a dominating solar induced cloud feedback we deduce a CO_2 climate sensitivity of $C_S = 0.7^\circ C$ and a solar sensitivity, related to 0.1% change of the solar constant, of $S_S = 0.17^\circ C$. The increase in the TSI over 100 years then contributes to a warming of 0.44°C (60%) and the 100 ppm increase of CO_2 over this period causes additional 0.30°C (40%) in excellent agreement with the measured warming and cloud cover.

Altogether, we see that the positive feedbacks, originating from clouds, water vapor, and albedo, are partially compensated or in the case of a moderate cloud feedback are even overcompensated by lapse rate and evaporation feedback. Particularly clouds have two stronger opposing effects on the energy balance, which can neutralize each other or can even have an overall attenuating impact on the ECS, dependent on the mechanisms responsible for cloud changes. From these studies we conclude that all constraints can best be explained by a cloud feedback mechanism, which is dominated by the solar influence, while thermally induced contributions only should have minor influence.

Our investigations further indicate that a CO_2 climate sensitivity larger than 1°C seems quite improbable, whereas a value of 0.6–0.8°C, depending on the considered solar anomaly, fits well with all observations of a changing solar constant, the cloud cover, and global temperature. A climate sensitivity as specified in AR5 (1.5–4.5°C) would only be possible when any solar influence could completely be excluded and the negative feedbacks further be attenuated.

Maybe the most important message of this investigation is that on the basis of well retraceable physical interrelations there exist several stronger arguments for the inclusion of some effects, which obviously were not considered in the IPCC reports and which can significantly attenuate the influence of CO_2 on global warming. The discrepancies primarily go back to an overall negative feedback we find in our calculation, and to the inclusion of solar effects.

Annex: Abbreviations. For further symbols, see also Table 6.

Abbreviations

2LCM:	two-layer climate model
AGW:	anthropogenic global warming
$\mathbf{a}_{LW}$:	long wave absorptivity (of CO_2, WV, CH_4, and O_3)
$\mathbf{a}_{SW}$:	short wave absorptivity (of CO_2, WV, and CH_4)
AR4:	Fourth Assessment Report of the IPCC (2007)
AR5:	Fifth Assessment Report of the IPCC (2013)
AOGCM:	atmosphere-ocean general circulation model
BEST:	Berkley Earth Surface Temperature
CMIP5:	Coupled Model Intercomparison Project Phase 5
C_C:	cloud cover
C_S:	equilibrium climate sensitivity
C_{WV}:	water vapor concentration
c_f:	temperature induced cloud cover parameter
ΔE_S:	solar anomaly over last century
δE_S:	solar anomaly over the eighties and nineties
EASy:	Earth-atmosphere system
ECS:	equilibrium climate sensitivity
f_A:	downward directed fraction of atmospheric radiation
$f_{WV}, f_{LR}, f_{SA}, f_{CO}, f_{EV}$:	feedbacks: WV, lapse rate, surface albedo, convection, and evaporation
f_{CT}, f_{CS}:	cloud feedbacks: thermally or solar induced
GCM:	general circulation model
GEWEX:	Global Energy and Water Cycle Experiment
GH gases:	greenhouse gases
GISS:	Goddard Institute for Space Studies

GPS:	global positioning satellite
CMIP5:	Coupled Model Intercomparison Project Phase 5
HadCRUT:	Hadley Centre and Climate Research Unit
h_C:	convection heat transfer coefficient
IPCC:	Intergovernmental Panel on Climate Change
ISCCP:	International Satellite Cloud Climatology Project
λ_S:	Planck sensitivity, climate sensitivity parameter
l_H:	latent heat transfer coefficient
lw radiation:	long wave radiation
MRT:	molecular response theory
SICF:	solar induced cloud feedback
OLR:	outgoing long wave radiation
PDO:	Pacific Decadal Oscillations
ppm, ppmv:	parts per million by volume
RF:	radiative forcing
RT calculations:	radiation transfer calculations
s_f:	solar induced cloud cover parameter
SICF:	solar induced cloud feedback
SOI:	Southern Oscillation Index
S_S:	solar sensitivity, temperature increase at 0.1% increase of TSI
sw radiation:	short wave radiation
T_A:	atmospheric temperature
T_E:	Earth (surface) temperature
T_R:	reference temperature (16°C)
TFK-scheme:	energy and radiation budget scheme after Trenberth et al. [21]
TOA:	top of the atmosphere
TICF:	thermally induced cloud feedback
TSI:	total solar irradiance
WV:	water vapor.

Competing Interests

The author declares that he has no competing interests.

Acknowledgments

The author thanks D. Grischkowsky from Oklahoma State University and W. Happer from Princeton University for very helpful discussions on spectral lineshape effects, W. Soon from Harvard-Smithsonian Center for Astrophysics for his valuable advice on solar and temperature correlations, and M. Salby, formerly Macquarie University Sydney, for his many constructive suggestions when preparing the paper.

References

[1] T. F. Stocker, D. Qin, G.-K. Plattner et al., Eds., *Climate Change 2013: The Physical Science Basis*, Cambridge University Press, New York, NY, USA, 2014.

[2] J. R. Petit, J. Jouzel, D. Raynaud et al., "Climate and atmospheric history of the past 420,000 years from the Vostok ice core, Antarctica," *Nature*, vol. 399, no. 6735, pp. 429–436, 1999.

[3] E. Monnin, A. Indermühle, A. Dällenbach et al., "Atmospheric CO_2 concentrations over the last glacial termination," *Science*, vol. 291, no. 5501, pp. 112–114, 2001.

[4] N. Caillon, J. P. Severinghaus, J. Jouzel, J.-M. Barnola, J. Kang, and V. Y. Lipenkov, "Timing of atmospheric CO_2 and antarctic temperature changes across termination III," *Science*, vol. 299, no. 5613, pp. 1728–1731, 2003.

[5] M. S. Torn and J. Harte, "Missing feedbacks, asymmetric uncertainties, and the underestimation of future warming," *Geophysical Research Letters*, vol. 33, no. 10, Article ID L10703, 2006.

[6] O. Humlum, K. Stordahl, and J.-E. Solheim, "The phase relation between atmospheric carbon dioxide and global temperature," *Global and Planetary Change*, vol. 100, pp. 51–69, 2013.

[7] M. Salby, Relationship between Greenhouse Gases and Global Temperature, video presentation, April 2013, Hamburg, Germany, https://www.youtube.com/watch?v=2ROw_cDKwc0.

[8] D. V. Hoyt and K. H. Schatten, "Group sunspot numbers: a new solar activity reconstruction," *Solar Physics*, vol. 179, no. 1, pp. 189–219, 1998.

[9] R. C. Willson and A. V. Mordvinov, "Secular total solar irradiance trend during solar cycles 21–23," *Geophysical Research Letters*, vol. 30, no. 5, pp. 1–4, 2003.

[10] A. Shapiro, W. Schmutz, E. Rozanov, M. Schoell, M. Haberreiter, and S. Nyeki, "A new approach to long-term reconstruction of the solar irradiance leads to large historical solar forcing," *Astronomy & Astrophysics*, vol. 529, article 67, 2011.

[11] S. Ziskin and N. J. Shaviv, "Quantifying the role of solar radiative forcing over the 20th century," *Advances in Space Research*, vol. 50, no. 6, pp. 762–776, 2012.

[12] N. Scafetta and R. C. Willson, "ACRIM total solar irradiance satellite composite validation versus TSI proxy models," *Astrophysics and Space Science*, vol. 350, no. 2, pp. 421–442, 2014.

[13] I. G. Usoskin, G. Hulot, Y. Gallet et al., "Evidence for distinct modes of solar activity," *Astronomy & Astrophysics*, vol. 562, article L10, 2014.

[14] X. Zhao and X. Feng, "Periodicities of solar activity and the surface temperature variation of the Earth and their correlations," *Chinese Science Bulletin*, vol. 59, no. 14, pp. 1284–1292, 2014.

[15] W. Soon, R. Connolly, and M. Connolly, "Re-evaluating the role of solar variability on Northern Hemisphere temperature trends since the 19th century," *Earth-Science Reviews*, vol. 150, pp. 409–452, 2015.

[16] H. Harde, "Advanced two-layer climatemodel for the assessment of global warming by CO_2," *Open Journal of Atmospheric and Climate Change*, vol. 1, no. 3, pp. 1–50, 2014.

[17] N. Lewis and M. Crok, *A Sensitive Matter—How the IPCC Buried Evidence Showing Good News about Global Warming*, The Global Warming Policy Foundation, 2014, http://www.thegwpf.org/content/uploads/2014/03/Oversensitive-download.pdf.

[18] H. Harde, "Radiation and heat transfer in the atmosphere: a comprehensive approach on a molecular basis," *International Journal of Atmospheric Sciences*, vol. 2013, Article ID 503727, 26 pages, 2013.

[19] H. Harde, *Was trägt CO_2 wirklich zur Globalen Erwärmung bei?: Spektroskopische Untersuchungen und Modellrechnungen zum Einfluss von H_2O, CO_2, CH_4 und O_3 auf unser Klima*, Books on Demand, Norderstedt, Germany, 2011.

[20] L. S. Rothman, I. E. Gordon, A. Barbe et al., "The HITRAN 2008 molecular spectroscopic database," *Journal Of Quantitative Spectroscopy and Radiative Transfer*, vol. 110, no. 9-10, pp. 533–572, 2008.

[21] K. E. Trenberth, J. T. Fasullo, and J. Kiehl, "Earth's global energy budget," *Bulletin of the American Meteorological Society*, vol. 90, no. 3, pp. 311–323, 2009.

[22] International Satellite Cloud Climatology Project (ISCCP), http://isccp.giss.nasa.gov/products/onlineData.html, Ole Humlum, http://www.climate4you.com/index.htm.

[23] H. Svensmark, "Influence of cosmic rays on Earth's climate," *Physical Review Letters*, vol. 81, no. 22, pp. 5027–5030, 1998.

[24] J. D. Haigh, "The impact of solar variability on climate," *Science*, vol. 272, no. 5264, pp. 981–984, 1996.

[25] F. Vahrenholt and S. Lüning, *Die Kalte Sonne*, Hoffmann und Campe, Hamburg, Germany, 2012.

[26] *Climate Change 2007: The Physical Science Basis. Contribution of Working Group I to the Fourth Assessment Report of the IPCC*, Climate Models and Their Evaluation, Section 8.6.3, Cambridge University Press, Cambridge, UK, 2007, http://www.ipcc.ch/publications_and_data/ar4/wg1/en/ch8s8-6-3-1.html.

[27] P. M. D. F. Forster and J. M. Gregory, "The climate sensitivity and its components diagnosed from earth radiation budget data," *Journal of Climate*, vol. 19, no. 1, pp. 39–52, 2006.

[28] R. S. Lindzen and Y.-S. Choi, "On the observational determination of climate sensitivity and its implications," *Asia-Pacific Journal of Atmospheric Sciences*, vol. 47, no. 4, pp. 377–390, 2011.

[29] D. R. Feldman, W. D. Collins, P. J. Gero, M. S. Torn, E. J. Mlawer, and T. R. Shippert, "Observational determination of surface radiative forcing by CO_2 from 2000 to 2010," *Nature*, vol. 519, no. 7543, pp. 339–343, 2015.

[30] K. Schwarzschild, "Über das Gleichgewicht in der solaren Atmosphäre—on the equilibrium of the sun's atmosphere," *Nachrichten der Koniglichen Gesellschaft der Wissenschaften zu Gottingen*, vol. 195, p. 41, 1906.

[31] K. Schwarzschild, "Diffusion and absorption in the sun's atmosphere," *Sitzungsberichte der Königlich Preussischen Akademie der Wissenschaften Berlin*, pp. 1183–1200, 1914.

[32] R. M. Goody and Y. L. Yung, *Atmospheric Radiation: Theoretical Basis*, Oxford University Press, 1989.

[33] M. L. Salby, *Physics of the Atmosphere and Climate*, Cambridge University Press, Cambridge, UK, 2012.

[34] S. Vey, *Bestimmung und Analyse des atmosphärischen Wasserdampfgehaltes aus globalen GPS-Beobachtungen einer Dekade mit besonderem Blick auf die Antarktis [Ph.D. thesis]*, Technical University Dresden, 2007.

[35] *U.S. Standard Atmosphere 1976*, National Oceanic and Atmospheric Administration, National Aeronautics and Space Administration, Washington, DC, USA, 1976.

[36] A. V. E. Ollila, "The roles of greenhouse gases in global warming," *Energy & Environment*, vol. 23, no. 5, pp. 781–799, 2012.

[37] D. L. Hartmann, *Global Physical Climatology*, Academic Press, New York, NY, USA, 1994.

[38] C. J. Stubenrauch, W. B. Rossow, S. Kinne et al., "Assessment of global cloud datasets from satellites: project and database initiated by the GEWEX radiation panel," *Bulletin of the American Meteorological Society*, 2013.

[39] G. Myhre, E. J. Highwood, K. P. Shine, and F. Stordal, "New estimates of radiative forcing due to well mixed greenhouse gases," *Geophysical Research Letters*, vol. 25, no. 14, pp. 2715–2718, 1998.

[40] H. Harde, N. Katzenellenbogen, and D. Grischkowsky, "Line-shape transition of collision broadened lines," *Physical Review Letters*, vol. 74, no. 8, pp. 1307–1310, 1995.

[41] H. Harde, R. A. Cheville, and D. Grischkowsky, "Terahertz studies of collision-broadened rotational lines," *Journal of Physical Chemistry A*, vol. 101, no. 20, pp. 3646–3660, 1997.

[42] H. Harde, R. A. Cheville, and D. Grischkowsky, "Collision-induced tunneling in methyl halides," *Journal of the Optical Society of America B: Optical Physics*, vol. 14, no. 12, pp. 3282–3293, 1997.

[43] H. Harde, J. Zhao, M. Wolff, R. A. Cheville, and D. Grischkowsky, "THz time-domain spectroscopy on ammonia," *Journal of Physical Chemistry A*, vol. 105, no. 25, pp. 6038–6047, 2001.

[44] H. Harde and D. Grischkowsky, "Molecular response theory in terms of the uncertainty principle," *Journal of Physical Chemistry A*, vol. 119, no. 34, pp. 9085–9090, 2015.

[45] D. E. Burch and D. A. Gryvnak, "Continuum absorption by H_20 vaper in the infrared and millimeter regions," in *Atmospheric Water Vapor*, A. Deepak, T. D. Wilkerson, and L. H. Ruhnke, Eds., Academic Press, New York, NY, USA, 1980.

[46] R. E. Roberts, J. E. A. Selby, and L. M. Biberman, "Infrared continuum absorption by atmospheric water vapor in the 8–12-μm window," *Applied Optics*, vol. 15, no. 9, pp. 2085–2090, 1976.

[47] D. P. Edwards and L. L. Strow, "Spectral line shape considerations for limb temperature sounders," *Journal of Geophysical Research*, vol. 96, no. D11, pp. 20859–20868, 1991.

[48] W. Happer, "Why has global warming paused?" *International Journal of Modern Physics A*, vol. 29, no. 7, Article ID 1460003, 2014.

[49] M. G. Mlynczak, T. S. Daniels, D. P. Kratz et al., "The spectroscopic foundation of radiative forcing of climate by carbon dioxide," *Geophysical Research Letters*, vol. 43, no. 10, pp. 5318–5325, 2016.

[50] N. Ozak, O. Aharonson, and I. Halevy, "Radiative transfer in CO_2-rich atmospheres: 1. Collisional line mixing implies a colder early Mars," *Journal of Geophysical Research: Planets*, vol. 121, no. 6, pp. 965–985, 2016.

[51] B. Barkstrom, E. Harrison, G. Smith et al., "Earth Radiation Budget Experiment (ERBE) archival and April 1985 results," *Bulletin of the American Meteorological Society*, vol. 70, pp. 1254–1262, 1985.

[52] T. D. Bess and G. L. Smith, "Earth radiation budget: results of outgoing longwave radiation from Nimbus-7, NOAA-9 and ERBS satellites," *Journal of Applied Meteorology*, vol. 32, no. 5, pp. 813–824, 1993.

[53] B. A. Wielicki, B. R. Barkstrom, E. F. Harrison, R. B. Lee III, G. L. Smith, and J. E. Cooper, "Clouds and the Earth's radiant energy system (CERES): an earth observing system experiment," *Bulletin of the American Meteorological Society*, vol. 77, no. 5, pp. 853–868, 1996.

[54] B. A. Wielicki, B. R. Barkstrom, E. F. Harrison et al., "CERES radiation budget accuracy overview," in *Proceedings of the 12th Conference on Atmospheric Radiation*, vol. 9.1, American Meteorological Society, Madison, Wis, USA, 2006.

[55] T. Wong, B. A. Wielicki, R. B. Lee III, G. L. Smith, K. A. Bush, and J. K. Willis, "Reexamination of the observed decadal variability of the earth radiation budget using altitude-corrected ERBE/ERBS nonscanner WFOV data," *Journal of Climate*, vol. 19, no. 16, pp. 4028–4048, 2006.

[56] K. P. Hoinka, "Statistics of the global tropopause pressure," *Monthly Weather Review*, vol. 126, no. 12, pp. 3303–3325, 1998.

[57] B. J. Soden and I. M. Held, "An assessment of climate feedbacks in coupled ocean-atmosphere models," *Journal of Climate*, vol. 19, no. 14, pp. 3354–3360, 2006.

[58] T. Andrews, P. M. Forster, and J. M. Gregory, "A surface energy perspective on climate change," *Journal of Climate*, vol. 22, pp. 2557–2570, 2009.

[59] J.-L. Dufresne and S. Bony, "An assessment of the primary sources of spread of global warming estimates from coupled atmosphere-ocean models," *Journal of Climate*, vol. 21, no. 19, pp. 5135–5144, 2008.

[60] A. C. Clement, R. Burgman, and J. R. Norris, "Observational and model evidence for positive low-level cloud feedback," *Science*, vol. 325, no. 5939, pp. 460–464, 2009.

[61] R. S. Lindzen, M.-D. Chou, and A. Y. Hou, "Does the earth have an adaptive infrared iris?" *Bulletin of the American Meteorological Society*, vol. 82, no. 3, pp. 417–432, 2001.

[62] B. A. Laken and E. Pallé, "Understanding sudden changes in cloud amount: the Southern Annular Mode and South American weather fluctuations," *Journal of Geophysical Research Atmospheres*, vol. 117, no. 13, pp. 1984–2012, 2012.

[63] H. Cho, C.-H. Ho, and Y.-S. Choi, "The observed variation in cloud-induced longwave radiation in response to sea surface temperature over the Pacific warm pool from MTSAT-1R imagery," *Geophysical Research Letters*, vol. 39, no. 18, Article ID L18802, 2012.

[64] P. M. Caldwell, Y. Zhang, and S. A. Klein, "CMIP3 subtropical stratocumulus cloud feedback interpreted through a mixed-layer model," *Journal of Climate*, vol. 26, no. 5, pp. 1607–1625, 2013.

[65] H. Svensmark, J. O. P. Pedersen, N. D. Marsh, M. B. Enghoff, and U. I. Uggerhøj, "Experimental evidence for the role of ions in particle nucleation under atmospheric conditions," *Proceedings of the Royal Society A: Mathematical, Physical and Engineering Sciences*, vol. 463, no. 2078, pp. 385–396, 2007.

[66] H. Svensmark, T. Bondo, and J. Svensmark, "Cosmic ray decreases affect atmospheric aerosols and clouds," *Geophysical Research Letters*, vol. 36, no. 15, pp. 1–4, 2009.

[67] M. B. Enghoff, J. O. P. Pedersen, U. I. Uggerhøj, S. M. Paling, and H. Svensmark, "Aerosol nucleation induced by a high energy particle beam," *Geophysical Research Letters*, vol. 38, no. 9, pp. 1–4, 2011.

[68] J. Kirkby, J. Curtius, J. Almeida et al., "Role of sulphuric acid, ammonia and galactic cosmic rays in atmospheric aerosol nucleation," *Nature*, vol. 476, no. 7361, pp. 429–435, 2011.

[69] Goddard Institute for Space Studies, http://data.giss.nasa.gov/gistemp/graphs.

[70] R. W. Spencer and W. D. Braswell, "On the misdiagnosis of surface temperature feedbacks from variations in Earth's radiant energy balance," *Remote Sensing*, vol. 3, no. 8, pp. 1603–1613, 2011.

[71] J. D. Haigh, "The role of stratospheric ozone in modulating the solar radiative forcing of climate," *Nature*, vol. 370, no. 6490, pp. 544–446, 1994.

[72] W. Soon, E. Posmentier, and S. Baliunas, "Climate hypersensitivity to solar forcing?" *Annales Geophysicae*, vol. 18, no. 5, pp. 583–588, 2000.

[73] J. D. Haigh, A. R. Winning, R. Toumi, and J. W. Harder, "An influence of solar spectral variations on radiative forcing of climate," *Nature*, vol. 467, no. 7316, pp. 696–699, 2010.

[74] J. E. Kristjánsson, J. Kristiansen, and E. Kaas, "Solar activity, cosmic rays, clouds and climate—an update," *Advances in Space Research*, vol. 34, no. 2, pp. 407–415, 2004.

[75] M. Voiculescu, I. G. Usoskin, and K. Mursula, "Different response of clouds to solar input," *Geophysical Research Letters*, vol. 33, no. 21, 2006.

[76] T. Wenzler, S. K. Solanki, and N. A. Krivova, "Reconstructed and measured total solar irradiance: is there a secular trend between 1978 and 2003?" *Geophysical Research Letters*, vol. 36, no. 11, Article ID L11102, 2009.

[77] M. Wild, D. Folini, C. Schär, N. Loeb, E. G. Dutton, and G. König-Langlo, "The global energy balance from a surface perspective," *Climate Dynamics*, vol. 40, no. 11-12, pp. 3107–3134, 2013.

[78] Ch. Monckton, W. W.-H. Soon, D. R. Legates, and W. M. Briggs, "Why models run hot: results from an irreducibly simple climate model," *Science Bulletin*, vol. 60, no. 1, pp. 122–135, 2015.

[79] H. Harde, "Scrutinizing the carbon cycle and CO_2 residence time in the atmosphere," *Global & Planetary Change*, In press.